UNIVERSITY OF VAASA

FACULTY OF TECHNOLOGY

TELECOMMUNICATION ENGINEERING

Toni Koskinen

UWB IN 3D INDOOR POSITIONING AND BASE STATION CALIBRATION

Master's thesis for the degree of Master of Science in Technology submitted for inspection, Vaasa, 15 Nov, 2010.

Supervisor	Professor Mohammed Salem Elmusrati
Instructor	M. Sc. (Tech.) Timo Lehikoinen

Acknowledgements

I am grateful to my instructor Timo Lehikoinen at the VTT Technical Research Centre of Finland who has given me the chance to participate in this research project and to all my colleagues for their assistance. I would like to thank my supervisor Professor Mohammed Elmusrati for my completion of the master's degree. And I also want to express my special gratitude to Dr. Tapio Heikkilä for his excellent guidance during my thesis work.

Lastly, I want to thank my parents for always supporting my personal and academic advancement and my girlfriend Sonja and her parents for their understanding and generosity.

TABLE OF CONTENTS

LIST OF ABBREVIATIONS

AM	Amplitude Modulation
AOA	Angle of Arrival
API	Application Programming Interface
AWGN	Additive White Gaussian Noise
BPM	Bi-Phase Modulation
CDF	Cumulative Distribution Function
CRLB	Cramer-Rao Lower Bound
CSS	Chirp Spread Spectrum
DAA	Detect And Avoid
DSSS	Direct Sequence Spreading Spectrum
DS-UWB	Direct Sequence Ultra Wideband
EC	European Commission
ECC	Electronic Communications Committee
EIRP	Equivalent Isotropically Radiated Power
FCC	Federal Communications Commission
FM	Frequency Modulation
GPS	Global Positioning System
ICI	Inter Channel Interference
IEEE	Institute of Electrical and Electronics Engineers
IR	Impulse Radio
ISI	Inter Symbol Interference
LDC	Low-Duty Cycle
LE	Location Engine
LOS	Line of Sight
LSQ	Least Squares Quadratic
MB-OFDM	Multiband OFDM
MIC	Ministry of Internal Affairs and Communications
NLOS	Non Line of Sight
OFDM	Orthogonal Frequency Division Multiplexing
OOK	On-off keying
OPM	Orthogonal Pulse Modulation
OTW	On the Wire
PAM	Pulse Amplitude Modulation
PHY	Physical Layer
PL	Path Loss
PN	Pseudo-Noise
POE	Power on Ethernet
PPM	Pulse Position Modulation
PR	Pseudo-Random
PSD	Power Spectral Density
RF	Radio Frequency

RSS	Received Signal Strength
RSSI	Received Signal Strength Indicator
RTLS	Real Time Location System
SNR	Signal to Noise Ratio
TDMA	Time Division Multiple Access
TDOA	Time-Difference of Arrival
TH-UWB	Time Hopping Ultra Wideband
TOA	Time of Arrival
TWR	Two-Way Ranging
UDP	User Datagram Protocol
ULA	Uniform Linear Array
UWB	Ultra Wideband
WLAN	Wireless Local Area Network
WPAN	Wireless Personal Area Network

UNIVERSITY OF VAASA
Faculty of technology
Author: Toni Koskinen
Topic of the Thesis: UWB in 3D Indoor Positioning and Base Station Calibration
Supervisor: Professor Mohammed Elmusrati
Instructor: Timo Lehikoinen
Degree: Master of Science in Technology
Department: Department of Computer Science
Degree Programme: Master's Degree in Telecommunication Engineering
Major of Subject: Telecommunication Engineering
Year of Entering the University: 2007
Year of Completing the Thesis: 2010 **Pages:** 84

ABSTRACT

There are several technologies available for object locating and tracking in outdoor and indoor environments but performance requirements are getting tighter and precise object tracking is still largely an open challenge for researchers. Ultra wideband technology (UWB) has been identified as one of the most promising techniques to enhance a mobile node with accurate ranging and tracking capabilities. For indoor applications almost all positioning technologies require physical installation of fixed infrastructure. This infrastructure is usually expensive to deploy and maintain. The aim of this thesis is to improve the accessibility of the RF-positioning systems by lowering the configuration cost.

Real time localisation and tracking systems (RTLS) based on RF technologies pose challenges especially for the deployment of positioning system over large areas or throughout buildings within a number of rooms. If calibration is done manually by providing information about the exact position of the base stations, the initial set-up is particularly time consuming and laborious. In this thesis a method for estimating the position and orientation (x, y, z, yaw, pitch and roll) of a base station of a real time localization system is presented. The algorithm uses two-dimensional Angle of Arrival information (i.e. azimuth and elevation measurements). This allows more inaccurate manual initial survey of the base stations and improves the final accuracy of the positioning.

The thesis presents an implementation of the algorithm, simulations and empirical results. In the experiments, hardware and software procured from Ubisense was used. The Ubisense RTLS bases on UWB technology and utilises Angle of Arrival and Time Difference of Arrival techniques. Performance and functionality of the Ubisense RTLS were measured in various radio environments as well as the implementation of the calibration algorithm. Simulations and experiment studies showed that camera calibration method can be successfully adapted to position systems based on UWB technology and that the base stations can be calibrated in a sufficient accuracy. Because of more flexible calibration, the final positioning accuracy of the Ubisense system was as whole in average better.

KEYWORDS: UWB, positioning, calibration, Ubisense

VAASAN YLIOPISTO

Teknillinen tiedekunta

Tekijä:	Toni Koskinen
Diplomityön nimi:	UWB 3D-sisätilapaikannuksessa ja Tukiaseman Kalibrointi
Valvojan nimi:	Professori Mohammed Elmusrati
Ohjaajan nimi:	Timo Lehikoinen
Tutkinto:	Diplomi- insinööri
Yksikkö:	Tieto- ja tietoliikennetekniikan yksikkö
Koulutusohjelma:	Master's Degree in Telecommunication Engineering
Suunta:	Tietoliikennetekniikka
Opintojen aloitusvuosi:	2007
Diplomityön valmistumisvuosi:	2010 **Sivumäärä:** 84

TIIVISTELMÄ

Sisätilapaikannukseen ei ole vielä löydetty joka tilanteeseen sopivaa ratkaisua. Paikannukseen tarkoitettuja teknologioita on useita, mutta tarkkuusvaatimukset ja tarkka kohteen seuranta vaativat tutkimusta. UWB-tekniikka (Ultralaajakaista) on yksi lupaavimpia kyseiseen tarkoitukseen. Sisätilapaikannuslaitteet vaativat yleensä kiinteän infrastruktuurin asennuksen. Tämä on yleensä kallista ja vaatii huoltoa. Työn tarkoituksena on parantaa paikannuslaitteistojen käytettävyyttä sekä alentamaan käyttö- ja kokoonpanokustannuksia.

Suuret ja moniosaiset tilat ovat haasteellisia radiotekniikkaan perustuville reaaliaikapaikannuslaitteille (RTLS). Jos kalibrointi tehdään manuaalisesti antamalla tarkat tiedot tukiasemien sijainneista, käyttöönotto on erityisesti aikaa vievää ja työlästä. Työssä esitetään vaihtoehtoinen kalibrointiin tarkoitettu algoritmi joka perustuu optisenkameran malliin. Algoritmi laskee tarkat arvot tukiaseman sijainnille (X, Y ja Z) ja asennolle (kääntyminen pituus-, pysty- ja poikkiakselin suhteen) sekä käyttää kaksiulotteista kulmamittaustietoa (vaaka- ja pystytaso). Tämä mahdollistaa vapaamman kalibroinnin epätarkemmalla manuaalisella sijaintimittauksella ja parantaa paikannuslaitteiston lopullista tarkkuutta.

Työssä käydään läpi yleisimpiä paikannusmenetelmiä UWB-tekniikalla, tutkitaan kalibrointialgoritmia sekä esitetään simulaatioita ja empiirisiä tuloksia. Mittauksissa käytetään Ubisensen paikannuslaitteistoa, joka perustuu UWB-tekniikkaan. Ubisense käyttää saapuvan signaalin kulma- (AOA) ja aikaero-estimointimenetelmiä (TDOA). Ubisensen tarkkuutta tutkittiin erilaisissa radioympäristöissä ja kalibrointialgoritmin toteuttamisessa. Simulaatiot ja mittaukset osoittivat, että kameran kalibrointimenetelmää voidaan soveltaa UWB-tekniikkaan perustuvassa paikannuslaitteistossa ja että tukiasemat voidaan kalibroida riittävällä tarkkuudella. Vapaampi kalibrointimenetelmä paransi laitteiston lopullista tarkkuutta.

AVAINSANAT: UWB, paikannus, kalibrointi, Ubisense

1. INTRODUCTION

In simple words, the idea behind the most accurate positioning systems under current development is estimating the time it takes of radio-wave to propagate from the transmitter to the receiver and converting that estimate to distance information to determine the *range* between the two devices. By calculating the range from the querying device to multiple devices it is possible to identify the position of a device itself (*positioning*). Finally, by keep calculating these range estimates over some time frame of a moving device inside an area covered by the positioning system, *tracking* can be enabled.

There are many obstacles in the detection and processing of the radio-wave signals, for example, constraints on the radio architecture (*standard and cost constraints*), constraints on the maximum power allowed in the air (*regulatory constraints*) and constraints on the maximum processing power (*technology constraints*).

Ultra wideband technology (UWB) has been identified as one of the most promising techniques to enhance a mobile terminal or a sensor with accurate ranging and tracking capabilities. Making correct use of UWB properties (such as bandwidth) has allowed the development of practical systems which today are offering ranging resolutions in the order of tens of centimetres and coverage of areas as large as hundreds of meters with a single set of UWB nodes.

Global Positioning System (GPS) is nowadays one of the most known positioning systems to broad public. The GPS requires communication with at least four GPS satellites, and offers location accuracy of several meters. It is used mainly for outdoor location-based applications, because its accuracy can degrade significantly in indoor scenarios. Wireless local area network (WLAN) technology has recently become a candidate technology for indoor localisation, but the location accuracy it offers is poor and often requires extensive preparatory manual surveying and calibration (e.g. fingerprinting) (Wang et al., 2003). WLAN's high power consumption of terminals is also an issue for power-sensitive mobile applications. Ultra wideband technologies promise to overcome power consumption and accuracy limitations of

both GPS and WLAN, and are more suitable for indoor location-based applications. (Ubisense, 2010; Time Domain, 2010)

There are several technologies available for object locating and tracking in outdoor and indoor environments but performance requirements are getting tighter and precise object tracking is still largely an open challenge for researchers. For indoor applications almost all of them require physical installation of fixed infrastructure. This infrastructure is usually expensive to deploy and maintain (Paul and Wan, 2009; Zhang, Partridge and Reich, 2007). The aim of this thesis is to improve the accessibility of the RF-positioning systems by lowering the configuration cost. Algorithms for calibrating a variety of systems using pseudoranging timing models and/or angle of arrival are presented and implemented.

The thesis is organised as follows. Chapter 2 provides UWB overview in positioning and data transmission. Chapter 3 overviews the most common positioning techniques used mainly in RF-systems. Chapter 4 provides measurements and results with UWB positioning system. Chapter 5 covers some calibration algorithms, simulations and results using real hardware deployment. Chapter 6 concludes the thesis with remarks.

2. UWB

Ultra wideband (UWB) is an untypical type of radio. Radio is a device sending and receiving electromagnetic signals between transmitters and receivers wirelessly. Radio requires transmitters for generating signals, and receivers to transform the received information. The transmitter's antenna converts the information into electromagnetic energy and at the receiver the antenna collects the energy. (Siwiak and McKeown, 2004)

Radio signals share the limited spectrum by reserving slices of spectrum that are as narrow as possible. A signal with no information has zero bandwidth. Figure 2.1 shows the electromagnetic spectrum. Each radio service has its own location in the spectrum, frequencies for wireless communication share the beginning of the spectrum and the end of the spectrum is for visible light and cosmic radiation. (Siwiak and McKeown, 2004)

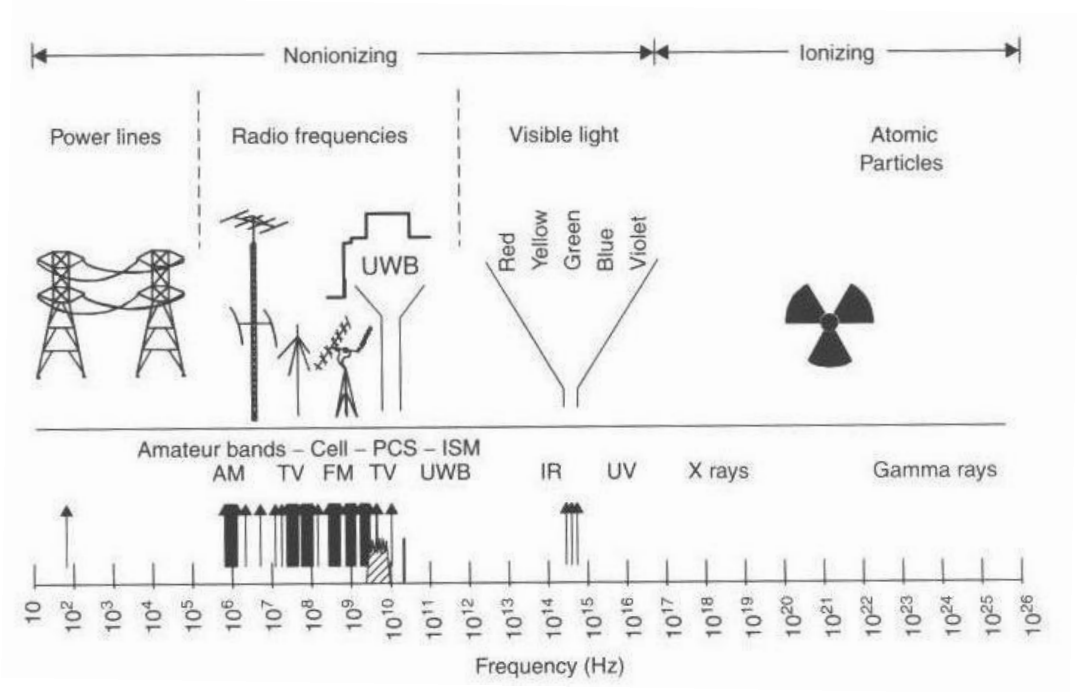

Figure 2.1. Radio services occupy unique locations in the spectrum (Siwiak and McKeown, 2004)

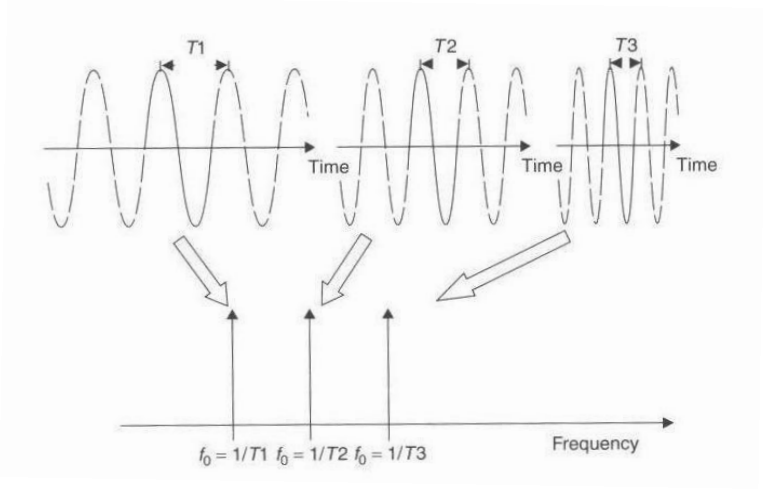

Figure 2.2. Different wavelengths of sines and cosines occupy unique spots in the spectrum (Siwiak and McKeown, 2004)

Figure. 2.2 has sinusoidal signals with different frequencies. Conventional radio signals can be discriminated one from other because they occupy unique locations in the radio spectrum.

Signals can be separated not only by bands, by channels and by frequencies but by time, especially in tiny slices of time. These short and ultrashort time slices occupy wide bandwidths and ultrawide bandwidths in the spectrum (see Fig. 2.3). The shorter the time, the wider is the bandwidth of the signal in the radio spectrum (see Fig. 2.4). It can also be seen that the entire frequency spectrum can be occupied by multiple users. In this case the users are separated in time rather in frequency. (Siwiak and McKeown, 2004)

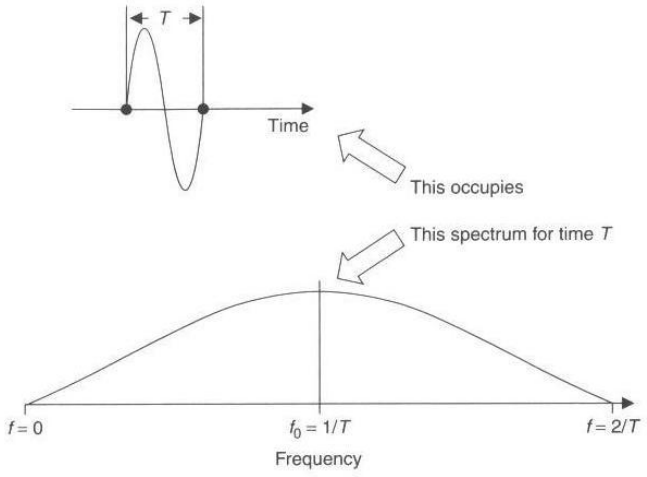

Figure 2.3. Length of signal in time occupies a spectrum width in frequency (Siwiak and McKeown, 2004)

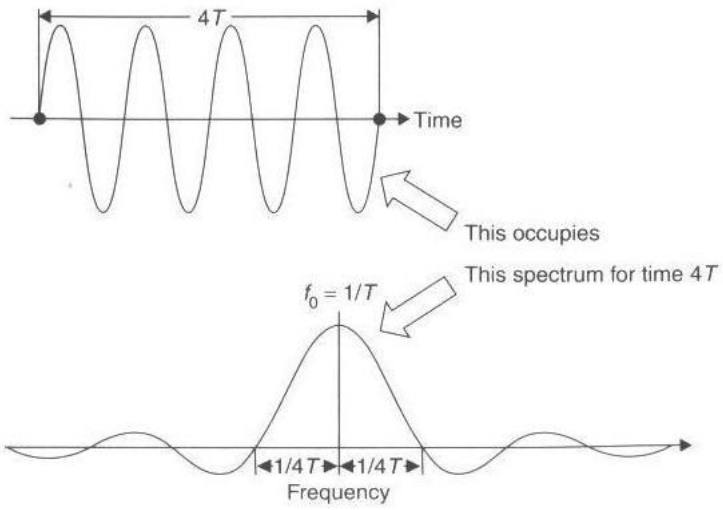

Figure 2.4. Signal in time domain occupies a bandwidth in frequency spectrum (Siwiak and McKeown, 2004)

2.1. Introduction

Originally Ultra Wideband (UWB) was used for radar, sensing, military communications and niche applications, but recently the world of UWB has changed dramatically, when the FCC (Federal Communications Commission, 2002a,b) issued that UWB could be used in data communications, radar and safety applications.

Ultra wideband is a very high bit rate Wireless personal area network (WPAN), previously under standardisation in IEEE 802.15.3a and recently approved by Ecma International in ECMA-368. The Ecma standard specifies a basis for high-speed and short-range WPANs, utilising part of the spectrum between 3.1 GHz and 10.6 GHz with data rates up to 480 Mbps. UWB can offer 50 to 500 times greater data rates compared to other WPAN radios, for example, Bluetooth. It is foreseen to replace high-speed cables and audio-video connections in homes and offices or be used for accurate location estimation for low data rate applications. One unique feature of UWB systems is their low average transmitted power. (ECMA International, 2008)

In addition to high-rate WPAN applications, UWB signals have also been considered for low-rate WPANs that concentrate on low power and low complexity devices. The IEEE formed a

task group 4a (TG4a) in March 2004 for revision to the IEEE 802.15.4 standard for an alternative PHY. The IEEE 802.15.4a provides high-precision ranging/localisation capability, high aggregate throughput and ultra-low-power consumption. The IEEE 802.15.4a specifies two optional signalling formats based on impulse radio (IR) UWB and chirp spread spectrum (CSS). The IR-UWB system can use 250 – 750 MHz,
3.244 – 4.742 GHz, or 5.944 – 10.234 GHz bands; whereas the CSS uses the 2.4 – 2.4835 GHz band. For the IR-UWB option, there is an optional ranging capability, whereas the CSS signals can only be used for data communication. (IEEE Computer Society, 2007)

The signal of UWB is very noise-like which makes interception and detection quite difficult. Due to its low spectral density, it should cause only very little interference to other systems.

UWB, which is sometimes referred as shared unlicensed system, coexists with other licensed and unlicensed narrowband systems. Because narrowband systems are affected from UWB signals, the transmission power of UWB devices has to be controlled. Regulatory agencies, such as, Federal Communications Commission (FCC) in United States, and Electronic Communications Committee (ECC) in Europe controls it. Therefore, UWB systems are allowed to coexist with other technologies within the same radio spectrum.

In current definition, any wireless communication technology that produces signals with a bandwidth wider than 500 MHz or a fractional bandwidth greater than 0.2 can be considered as UWB. The fractional bandwidth can be determined as

$$B_f = 2\frac{f_H - f_L}{f_H + f_L} \tag{2.1}$$

where f_L is the lower and f_H is the higher -10 dB point in a spectrum. (FCC , 2002)

2.2. Spectral Masks

The spectrum of the UWB is one of the major issues when regulating the UWB standards. Power output in certain frequencies is controlled and regulated to prevent interference to other devices nearby of the same frequencies. Because the UWB covers a large spectrum it is possible that it interferes with other systems. To prevent this interference, the FCC and other regulatory groups specify spectral masks for different applications. These masks show the allowed power output for specific frequencies.

2.2.1. UWB Regulation in USA

In February 2002, the FCC defined the FCC UWB rulings that provided the first radiation limitations for the UWB, technology commercialization was also permitted. The allowed mean EIRP (Equivalent Isotropically Radiated Power) transmission power was regulated to -41.25 dBm / MHz in the 3.1 – 10.6 GHz spectrum (see Table 2.1 and Fig. 2.5). (FCC , 2006)

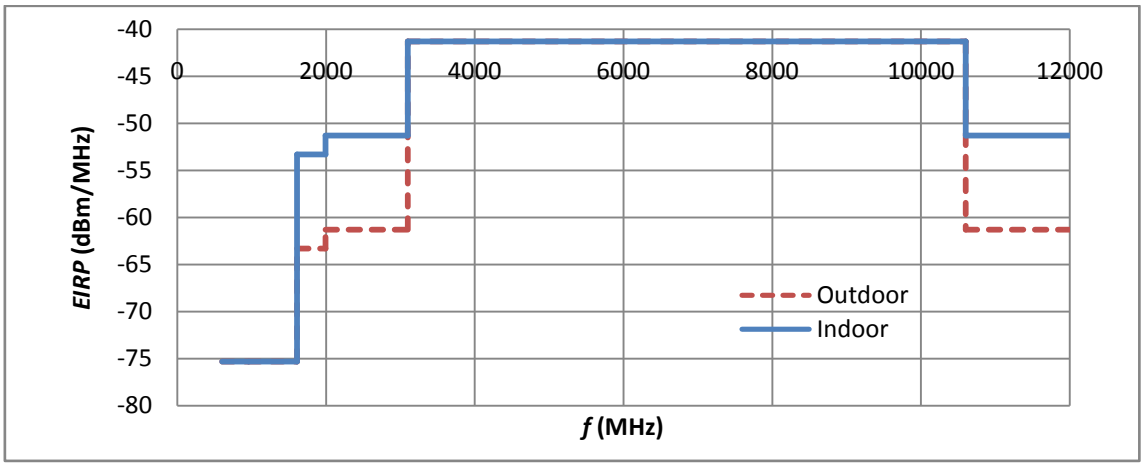

Figure 2.5. Spectral mask for UWB, mandated by FCC

Table 2.1. The FCC radiation limits for communication applications

Frequency (MHz)	*Indoor, EIRP(dBm)*	*Outdoor, EIRP (dBm)*
960–1610	-75.3	-75.3
1610–1990	-53.3	-63.3
1990–3100	-51.3	-61.3
3100–10600	-41.3	-41.3
Above 10600–	-51.3	-61.3

2.2.2. UWB Regulation in Europe

In February 2007, the European Commission (EC) approved the use of UWB spectrum. The EC chose only part of spectrum that was used in the US. The allowed mean EIRP transmission power -41.3 dBm / MHz was applied over the 6.0 – 8.5 GHz frequency range. It is also applied provisionally until the end of 2010 in the 4.2 – 4.8 GHz range (see Table 2.2 and Fig. 2.6). (Commission of the European Communities, 2007)

Table 2.2. The EC radiation limits for communication applications

Frequency range (MHz)	*Maximum mean EIRP density (dBm/MHz)*	*Maximum peak EIRP density (dBm/50MHz)*
Below 1600	-90.0	-50.0
1600–3400	-85.0	-45.0
3400–3800	-85.0	-45.0
3800–4200	-70.0	-30.0
4200-–4800	-41.3 *(until Dec 31, 2010)* – 70.0 *(beyond Dec 31, 2010)*	0.0 *(until Dec31, 2010)* – 30.0 *(beyond Dec 31, 2010)*
4800-6000	-70.0	-30.0
6000-8500	-41.3	0.0
8500-10600	-65.0	-25.0
Above 10600	-85.0	-45.0

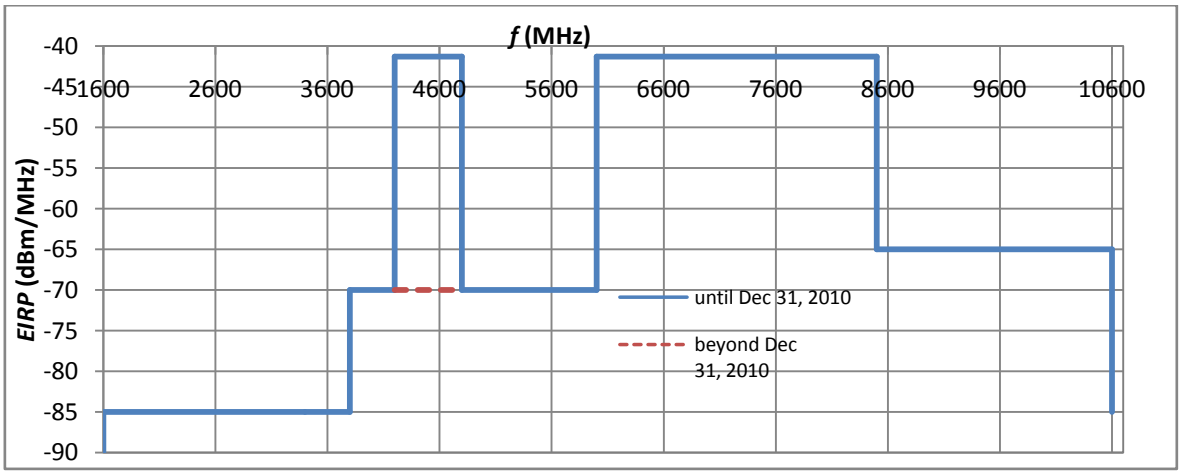

Figure 2.6. Spectral mask for UWB, mandated by EC

2.2.3. UWB Regulations World Widely

International regulations for UWB spectrum in indoor usage have been lately authorised. The Figure 2.7 shows spectral masks for UWB mandated by some of the organisations. The allowed radiation limits for the bands are mean EIRP transmission power -41.3 dBm / MHz where some of the bands require Detection and Avoid (DAA) techniques.

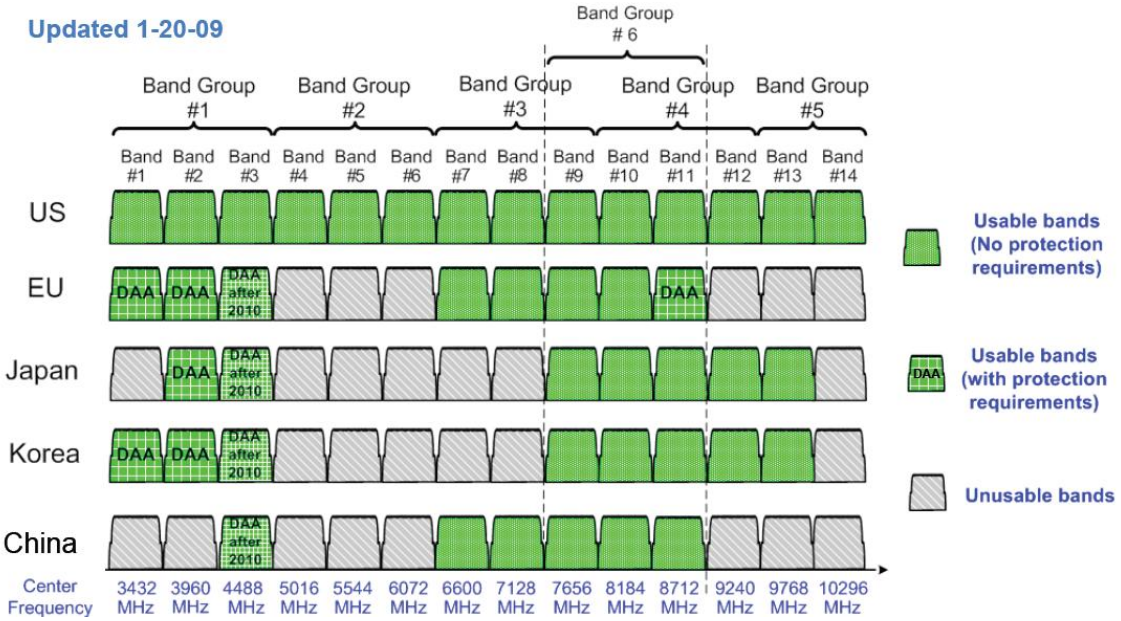

Figure 2.7 UWB Regulations **a**pproved by different governments (Wimedia Alliance, 2009).

2.3. Basic Properties of UWB Signals

Ultra wideband systems are characterized as systems with instantaneous spectral occupancy larger than 500 MHz, or with a bandwidth greater than 20% of the central frequency. (Arslan, Chen and Di Benedetto, 2006: 2)

The basic concept of the UWB is that frequency is meaningless; UWB systems use electromagnetic pulses instead of short-wave packets.

2.3.1. Pulse Shape

A typical pulse shape is sometimes known as a *Gaussian doublet,* which is shown in Figure 2.8. It is used often in UWB systems because its shape is easily generated. It is a square pulse shaped by rise and fall times. The filtering effects of antennas also round the edges.

Fast on and off switching leads to a pulse shape which is not rectangular, but has edges rounded (see Fig. 2.9). The Gaussian function *G(x)* fits the equation

$$G(x) = \frac{1}{\sqrt{2\pi\sigma^2}} e^{-x^2/\sqrt{2\sigma^2}} \qquad (2.2)$$

where σ is assumed to be zero mean. (Ghavami, Michael and Kohno, 2004: 9-11)

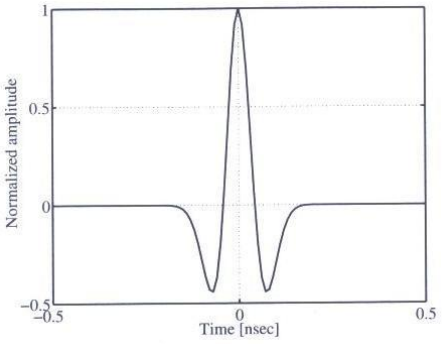

Figure 2.8. Idealized received UWB pulse shape

2.3.2. Pulse Trains

When transmitting information or data it needs to be modulated. In UWB, a single pulse does not carry much information, therefore it should be modulated onto a sequence of pulses, which is called as *pulse train.*

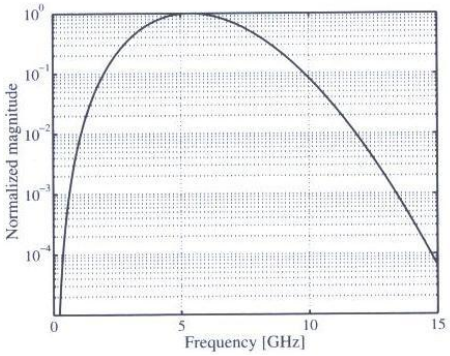

Figure 2.9. Idealized spectrum of a single received UWB pulse

When pulses are transmitted at regular intervals, the resulting spectrum contains peaks of power at certain frequencies. Because of the regulations on maximum transmit power, these peaks limit the total excess power. The spectrum can be made more noise-like by adding some random offset to each pulse or delaying or offsetting the pulse. By making this delaying cyclic according to a to a known *pseudo-noise* (PN) code, information can be modulated onto a pulse waveform. This is known as *pulse position modulation* (PPM). Modulation techniques are presented in Section 2.6. An unmodulated pulse train having a regular pulse output can be expressed as

$$s(t) = \sum_{n=-\infty}^{\infty} p(t - nT) \tag{2.3}$$

where $s(t)$ is a pulse train, $p(t)$ is the basis of pulse and *T* is the period. (Ghavami, Michael and Kohno, 2004: 12)

2.3.3. Multipath Propagation

For the positioning it is ideal to understand the concept of multipath propagation, particularly in an indoor wireless channel. Because of the extremely short UWB pulse width, the effects of multipath, such as *inter-symbol interference* (ISI) can be weakened.

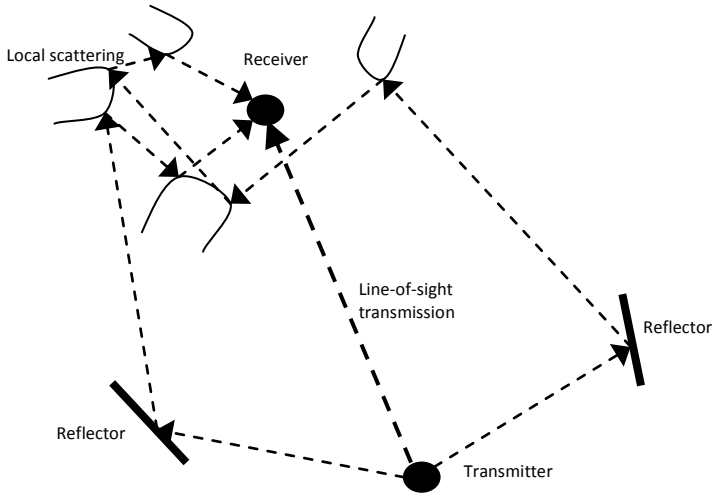

Figure 2.10. Indoor UWB radio multipath channel model

Multipath propagation is the name given to the phenomenon at the receiver whereby after the transmission of an electromagnetic signal propagates by various paths to the receiver. Figure 2.10 shows an example of a multipath propagation in a room. This effect is caused by reflection, absorption, diffraction and scattering of the signal by the objects between the transmitter and the receiver. Due to the lengths of different paths, pulses will arrive at the receiver at different times.

It can be seen that if pulses arrive within one pulse width they will interfere, while if they are separated by at least one pulse width they will not interfere. Because UWB signal's pulse width

is very narrow the odds of overlapping is low. Therefore UWB systems are often characterized as multipath resistant. (Ghavami, Michael and Kohno, 2004: 17-18)

2.3.4. Power Spectral Density

The power spectral density (PSD) of UWB systems is considered to be extremely low. The PSD is defined as

$$PSD = \frac{P}{B} \tag{2.4}$$

Where *P* is the power transmitted in watts (W), *B* is the bandwidth of the signal in hertz (Hz), and the unit of PSD is watts/hertz (W / Hz).

Most of the systems in wireless communication use a narrow bandwidth and can have a relatively high power spectral density. In today's consumer electronics the energy used should be as low as possible. If there is a fixed amount of energy, it can be either transmitted with a high amount of energy density over a small bandwidth or a very small amount of energy density over a large bandwidth. This mentioned comparison is shown in Figure 2.11. In UWB systems the energy is spread over a very large bandwidth, which derives to its name. The total amount of power can be calculated as the area under a frequency-power spectral density gap. The power spectral density of UWB communication systems in considered to be extremely low. (Ghavami, Michael and Kohno, 2004: 8)

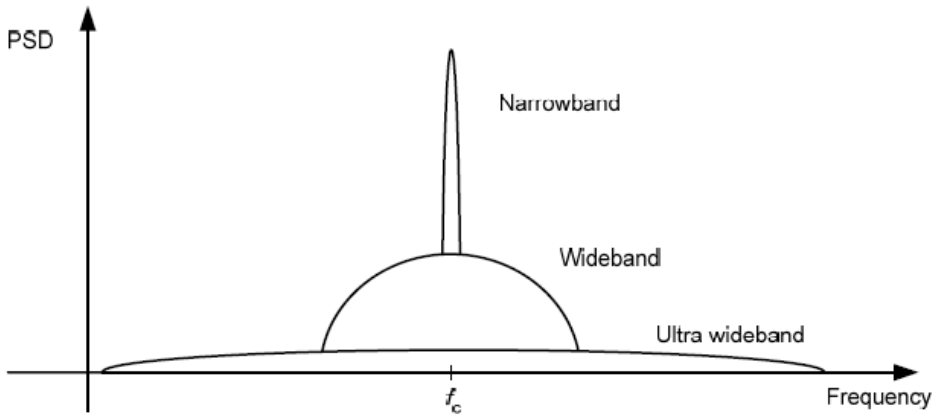

Figure 2.11. Power spectral densities over different bandwidths. (Hämäläinen, 2006: 26)

2.3.5. UWB and Shannon's Theory

The main advantage of UWB can be summarized by examining Shannon's capacity equation. Capacity is important as multimedia applications require higher and higher bit rates. The equation is expressed as

$$C = B \log\left(1 + \frac{S}{N}\right) \tag{2.5}$$

where *C* is the maximum channel capacity, with units [bits/second]; *B* is the channel bandwidth [Hz]; *S* is the signal power in watts [W] and *N* is the noise power also in watts. The equation shows that there are three things what can be done to increase the capacity of the channel. The signal power can be increased or the noise can be decreased. As it can be seen, the increase of bandwidth increases the capacity linearly, but the increase of signal power only increases it logarithmically, thus, it is more efficient to increase the bandwidth than the signal power. (Immoreev and Sinyavin, 2002: 4)

2.4. UWB Systems

Basically there are two types of UWB-technologies; Impulse Radio (IR) and Multiband OFDM. IR is based on transmitting extremely short and low power pulses. It is advantageous in that it eliminates the needs for up- and down-conversion and allows low-complexity transceivers. Multiband (or Multicarrier) modulation which can be done using Orthogonal Frequency Division Multiplexing (OFDM) has become popular technology due to its robustness against multipath interference and other special features. (Arslan, Chen and Di Benedetto, 2006: 2)

2.4.1. Singleband UWB

Singleband UWB technology is based on preceding Ultra wideband impulse radio technology, which name is still referred. The principle is to send the information in the whole spectrum in

very short pulses, less than nanosecond. The pulses are modulated by using the common modulation methods, such as, PPM, PAM, OOK and BPM.

There are two types of singleband UWB technologies; *Time Hopping Ultra Wideband* (TH-UWB) and *Direct Sequence Ultra Wideband* (DS-UWB). In TH-UWB the information pulses are transmitted in arbitrary intervals in slivers of time-axel defined by the pseudo-random code (Fig 2.12). TH-UWB needs precise timing, therefore both the transmitter and receiver needs to be synchronized precisely, so that the signal can be transmitted and received in its correct form.

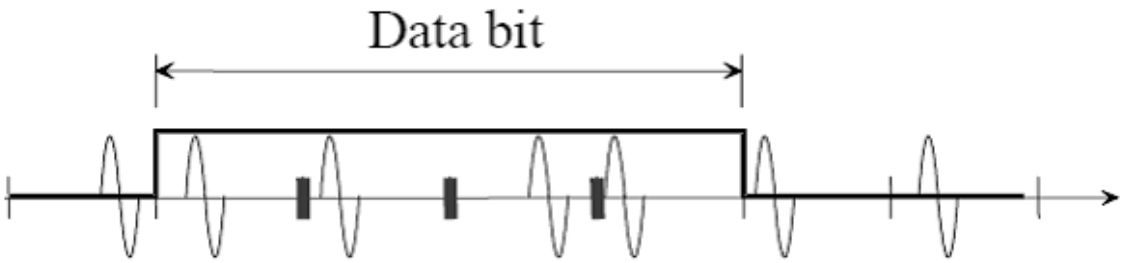

Figure 2.12. Time-Hopping Ultra Wideband

The concept of DS-UWB is similar to DSSS-signals. One data bit is spread into multiple chips. In DS-UWB the pulses are transmitted as a continuously pulse train, therefore its duty cycle is 100% (see Fig 2.13).

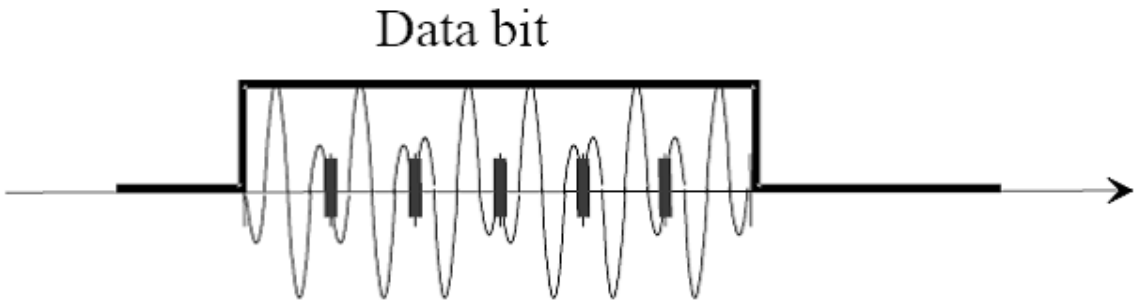

Figure 2.13. Direct Sequence Ultra Wideband

The disadvantage of DS-UWB is that is susceptible to interference between symbols (Inter Symbol Interference, ISI) and channels (Inter Channel Interference, ICI). This occurs from repetitive pulse transmission when reflections and delays of pulses cause faults in receiving.

Singleband UWB uses wider bandwidth so it suits well for environments with multipath propagation. (Oppermann, Hämäläinen and Iinatti, 2004)

2.4.2. Multiband UWB Impulse Radio

The use of wide spectrum made companies to develop Ultra wideband. To increase the efficient of transmission speed a system was developed where the information is sent simultaneously in multiple bands. This was named as Multiband UWB.

In multiband UWB, the frequency spectrum is divided into bands with bandwidth of at least 500 MHz by regulations of FCC. Each band can use its own modulation method and power level and occurrence is not dependent on other channels. Signals do not interfere each other, because they operate on different frequencies by the limits of UWB spectrum. For example, ten-band multiband UWB spectrum and signals (Fig. 2.14, 2.15). When transmitting simultaneously in all of the bands, higher transfer speed can be achieved compared to singleband UWB. The bands can also be used for OFDM, which makes possible to have multiple users at the same time in different channels. (Discrete Time Communications, 2002)

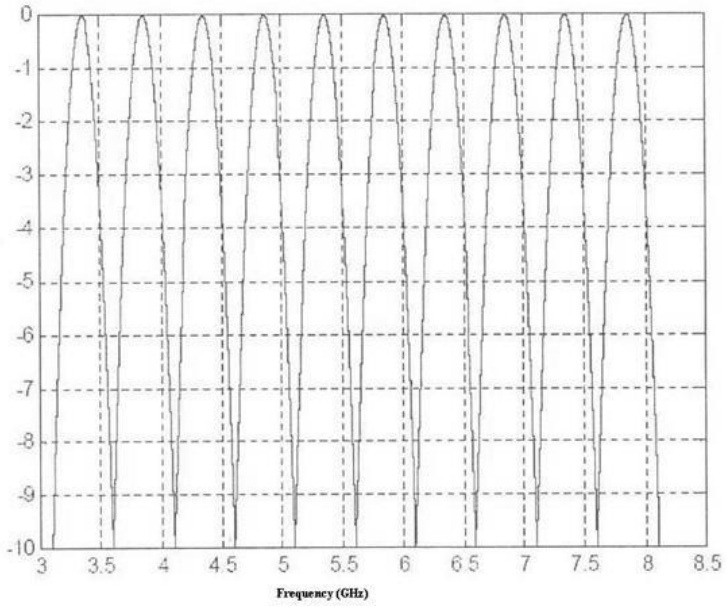

Figure 2.14. Spectrum of MB-UWB impulse radio (Discrete Time Communications, 2002)

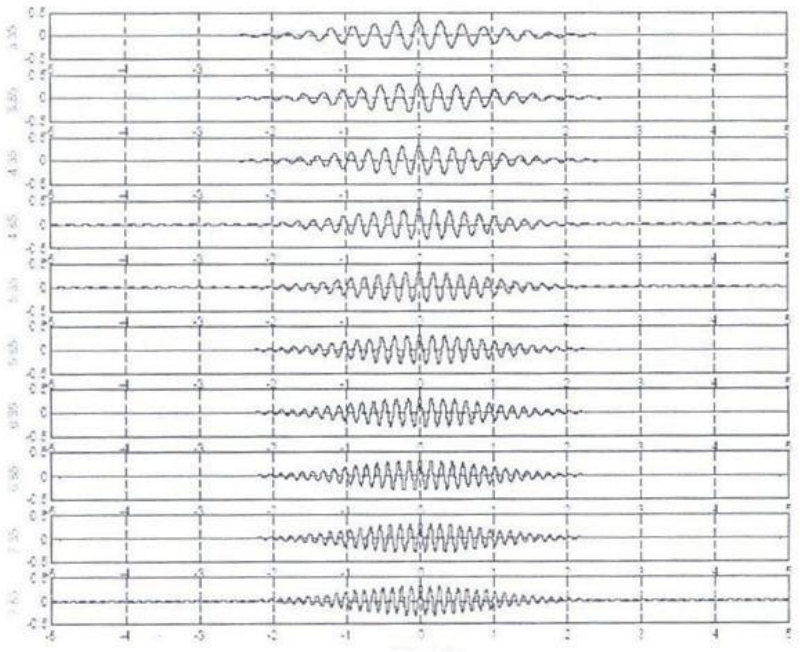

Figure 2.15. Signals of MB-UWB impulse radio (Discrete Time Communications, 2002)

The advantage of Multiband UWB is its flexibility and scalability. If necessary low speed rates can be used by using only few bands. By the usage of bands interference from other systems, such as, WLAN can be avoided and also interference to other systems can be avoided by leaving the certain operating channel away. (Discrete Time Communications, 2002)

2.4.3. Multiband OFDM

The basic idea of Multiband OFDM is to split the total available bandwidth into multiple frequency bands (Fig. 2.16). That is done by transmitting multiple UWB signals at different frequencies. Because the transmission is close to orthogonal over each of these bands, the signals do not interfere with each other. Figure 2.17 illustrates the channels of MB-OFDM.

By breaking the spectrum into pieces, a better co-existence with other current and future technologies can be achieved. As the spectral allocation is different in various parts of the world, worldwide interoperability of the UWB devices can be approached by using this method. Another advantage of multiband is the ability to avoid narrowband interference over

the frequency spectrum where strong interferers exist. (Arslan, Chen and Di Benedetto, 2006: 83)

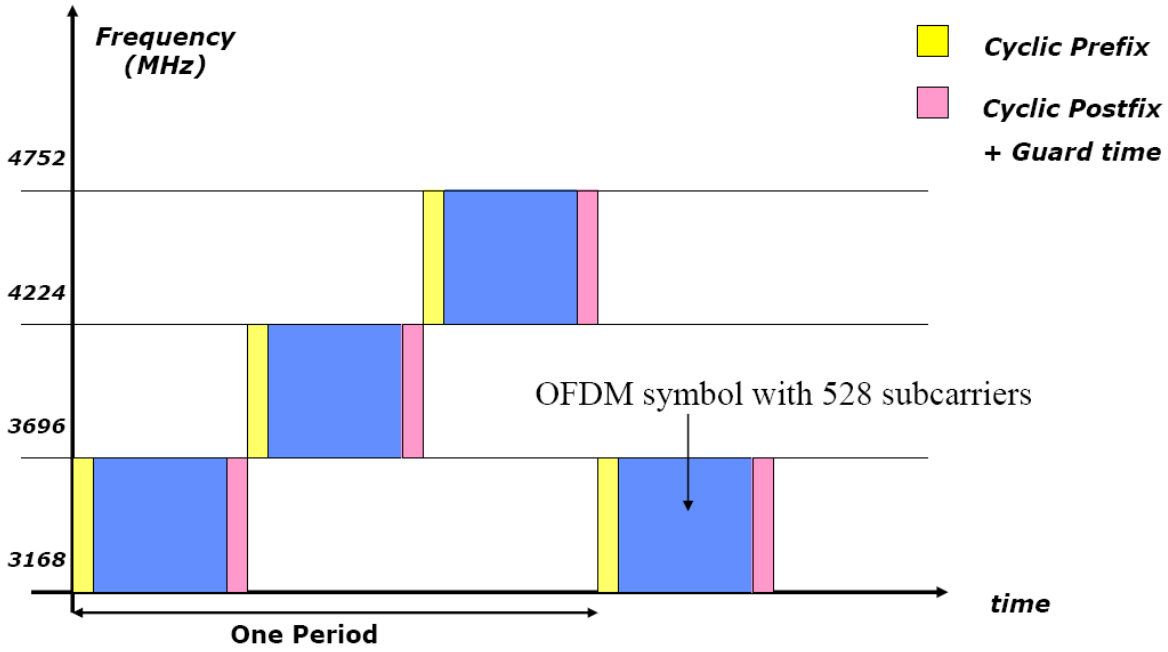

Figure 2.16. Principle of MB-OFDM (Svensson, 2004)

One of the advantages of OFDM is its transmission speed. In a relatively narrow bandwidth a lot of bits can be fitted by transmitting simultaneously multiple signals in different sub channels with overlapping frequencies. The name, multicarrier modulation is also used for this technique. Other advantages of OFDM are its immunity to multipath propagation and fault control. The disadvantage of OFDM is the transmitter complexity because the transmission uses the inverse Fourier transform. Multiband OFDM also uses more energy than the Multiband UWB impulse radio. (Arslan, Chen and Di Benedetto, 2006)

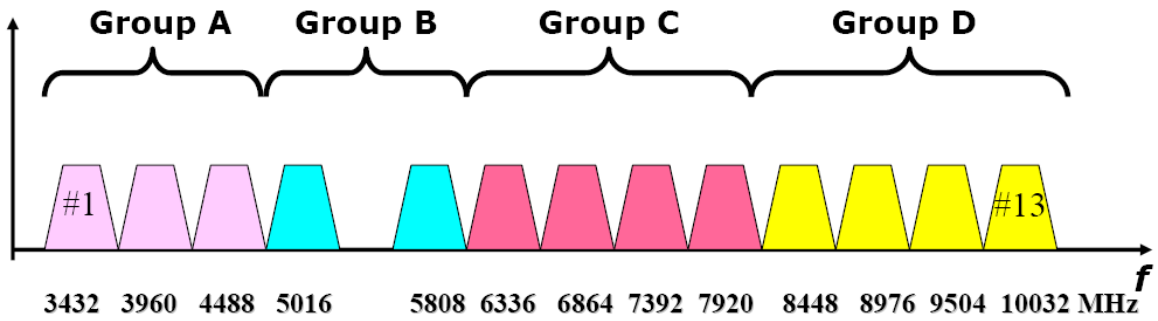

Figure 2.17. The channels of MB-OFDM (Svensson, 2004)

2.5. Modulation

Modulation is a procedure where information is manipulated on a carrier wave by changing some of the characteristics of the wave, such as amplitude, frequency or phase in conventional radio systems. A single pulse does not contain a lot of information. Selecting the appropriate modulation method in the UWB systems still remains major challenge. There are numerous modulations possible that depend on many factors, therefore it is crucial to choose the right modulation to right purpose (see Fig. 2.18).

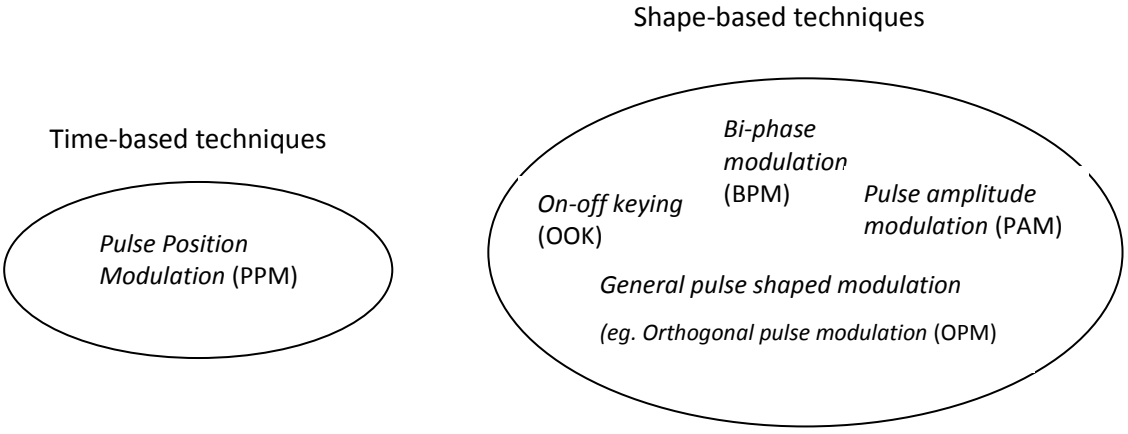

Figure 2.18. Common modulation techniques for UWB

2.5.1. UWB Modulation

The most used method modulation is *Pulse Position Modulation* (PPM) where each pulse is delayed or sent in advance. Another common method of modulation is *Bi-Phase Modulation*

(BPM). The idea is to invert the pulse by creating a pulse with opposite phase. Other known modulation techniques are available. For example, *On–Off keying* (OOK) where the absence or presence of a pulse signifies of “0” or “1”. (Ghavami, Michael and Kohno, 2004: 126)

In conventional radio frequency systems widely used *frequency modulation* (FM) cannot be used in UWB systems, because UWB pulses contains many frequency elements making it difficult to modulate. One popular modulation method in RF–systems is *Amplitude Modulation* (AM). Closely relate way to modulate is *Pulse Amplitude Modulation* (PAM) that is a technique where the amplitude of the pulse varies to contain digital information. (Ghavami, Michael and Kohno, 2004: 126)

2.5.2. Pulse Position Method

In PPM, the signal is delayed or sent advance to represent “1” and “0”. When defining a basic pulse to *p(t),* the delay to τ_i , and created pulse to S_i , we get the following equation:

$$s_i = p(t - \tau_i) \tag{2.6}$$

As an example we can let $\tau_1 = -0.75, \tau_2 = -0.25, \tau_3 = 0.25 \text{ and } \tau_4 = 0.75$ to create a 4–ary system PPM system. After assigning the values it can be seen that modulation shifts the pulse on the time axis. The advantages are simplicity and the ease how the delay may be controlled. For disadvantage the time control has to be extremely accurate. (Ghavami, Michael and Kohno, 2004: 128)

Figure 2.19. Pulse Position Modulation

2.5.3. Bi-Phase Modulation

In Figure 2.20 it can be seen that by using the BPM information the information can be made by inverting pulse, therefore it can be defined as a shape modulation. To simplify the explanation, we can describe the modulation as

$$s_i = \sigma_i p(t), \qquad \sigma_i = 1, -1 \tag{2.7}$$

where *p(t)* is the basic pulse and σ is a shape parameter and is known as the pulse weight. Assuming a binary system, the two resultant pulse shapes S_i and S_i can be defined as simply as $S_1 = p(t)$ and $S_2 = -p(t)$.

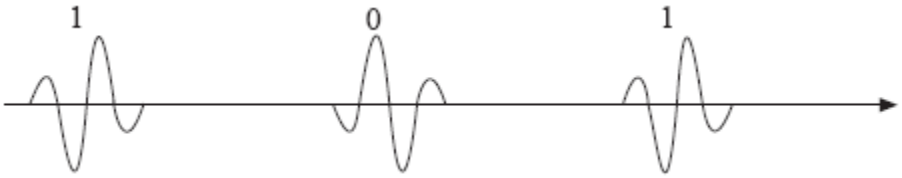

Figure 2.20. Bi-Phase Modulation

The advantages of BPM are 3 dB gain in power efficiency and the mean of σ is always zero. This allows removing the spectral peaks in some conditions. If PPM delays pulses by one pulse width, it can send twice more pulses at the same time. (Ghavami, Michael and Kohno, 2004: 129)

Though previously mentioned PPM and BPM are the most popular modulation techniques, other techniques have been proposed and can be used. Modulation methods for UWB are summarized in Table 2.4.

Table 2.3 Advantages and disadvantages of some UWB modulation methods

Method	*Advantages*	*Disadvantages*
BPM	Simplicity, efficient	Only for binary systems
OOK	Simplicity	Binary only, noise immunity
OPM	Orthogonal for Multiple access	Complexity
PAM	Simplicity	Noise immunity
PPM	Simplicity	Needs time resolution

2.6. UWB Transmitter and Receiver Structures

In telecommunication, both the receiver and the transmitter are needed. Usually a word *transceiver* is used when a device is capable of transmitting and receiving signals. Due to UWB signals' noise-likeness, the receiving or even detection is more difficult than in conventional RF systems, but on the other hand it makes the information security better.

Impulse radio UWB systems have relatively low complexity and therefore low cost. The circuits can be characterized as "all-digital", and mixers or amplifiers are not needed like in conventional radio systems.

The antennas play an important role in UWB system designing, due to low power of UWB signals and their pulse-shaping features.

2.6.1. UWB Transmitter

UWB transmitter is a circuit which converts significant data that is going to be transmitted into symbols and then modulates the symbols stream and passes the stream through a pulse generator to antenna. Pulses can be amplified, but to meet the power spectral requirements, large gain is not needed. A block diagram of UWB transmitter is shown in Figure 2.21 (Ghavami, Michael and Kohno, 2004: 137)

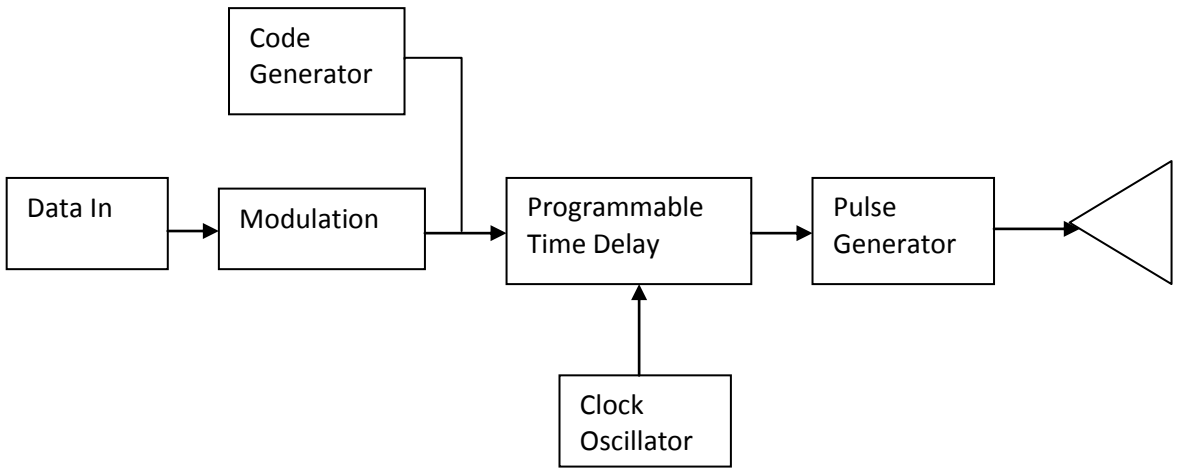

Figure 2.21. Simplified block diagram of a UWB transmitter

2.6.2. UWB Receiver

The UWB receiver is more complicated than a transmitter (see Fig. 2.22). It basically performs the opposite operation of the transmitter to recover the data and passes the data to any application requiring it.

When receiving requested UWB pulses, the wanted pulses must be detected or acquisitioned for locating the wanted pulses. These pulses must be traced continuously to compensate for any errors between the clocks in the receiver and transmitter, because the differences in temperature and manufacturer cause oscillators to become slightly faster or slower, and that causes receiver to be unable to demodulate the pulses. (Ghavami, Michael and Kohno, 2004)

The correlator in the receiver multiplies the received signal by a template waveform and then integrates the output to a DC–voltage. This happens in less than a nanosecond. For example, if the received data is modulated by using the PPM, the correlator detects the synchronization of the pulse. As for a simple example, if the received pulse is ¼ of a pulse early the output of the correlator is +1 and when the received pulse is ¼ of a pulse late, the output would be -1. When the pulse arrives centered, the output is zero. (Ghavami, Michael and Kohno, 2004)

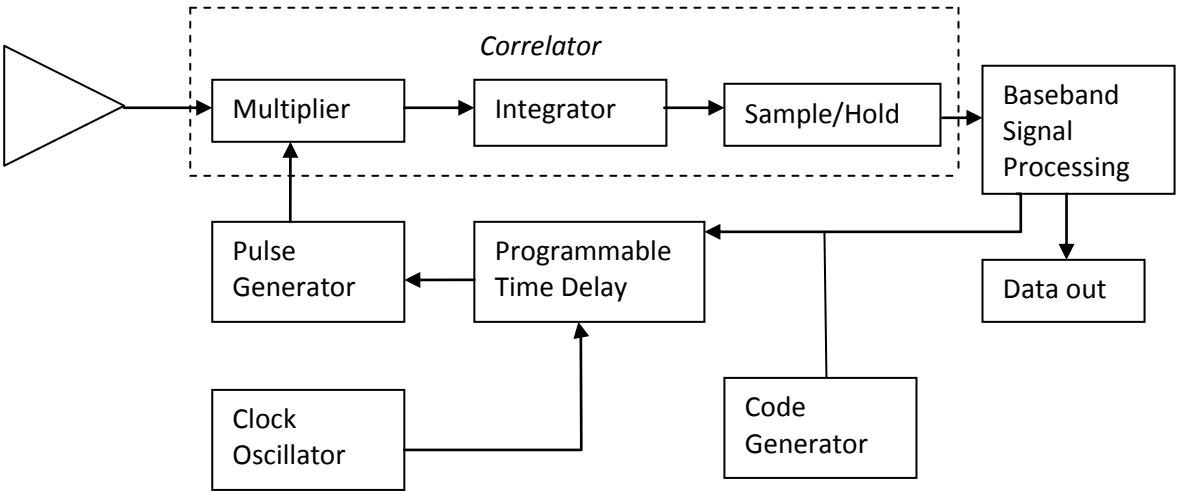

Figure 2.22. Block diagram of a PulsOn UWB receiver

2.7. Advantages of UWB

UWB has several advantages that make it suitable and interesting for consumer communications applications. The main benefits of UWB systems are high data rate, low complexity and hence low cost, a noise-like signal, a resistance to severe multipath and jamming and also very good time domain resolution for localisation applications. The low cost and complexity is explained by the nature of UWB signal. The UWB transmitter produces a very short time domain pulse, which can propagate without an additional *radio frequency* (RF) mixing stage, up-conversion and amplification.

Because of the low energy density and *pseudo-random* (PR) characteristics of the transmitted signal, the UWB signal is noise-like. This causes the unintended detection quite difficult, the transmissions also should not cause interference with other existing radio systems.

Due to large bandwidth of the UWB transmission signal, multipath propagation achieves very high resolution. The large bandwidth offers great frequency diversity, which makes the signal resistant to multipath propagation and interference when the transmission is discontinuous.
A penetration capability of a UWB signal is a result of its large frequency spectrum that includes low frequencies as well as high frequencies.

The large spectrum also results in high time resolution (or extremely narrow time domain pulses), which improves the ranging accuracy. The UWB radios are able to offer much better timing precision than, for example, GPS (Global Positioning System) and other narrowband radio systems. (Sahinoglu, Gezici and Güvenc, 2008)

3. WIRELESS POSITION ESTIMATION TECHNIQUES

This chapter focuses on position estimation techniques from a UWB perspective. In order to estimate the position of a node in a wireless network, signals are exchanged between the target node and a number of reference nodes by measuring a set of signal parameters. Depending on accuracy requirements, various signal parameters can be employed. In general, a single parameter is estimated for each received signal, for example, the arrival time of the signal. However, multiple signal parameters can be estimated in order to improve the positioning accuracy.

3.1. Angle of Arrival

The Angle of Arrival (AOA) is a measurement method to determine the direction of an incoming signal, which is the angle between two nodes. Generally, the AOA is determined by utilising individual elements of an antenna array. The angle information is obtained by measuring the differences of the incoming signal to different antenna elements, for example, time difference (or phase for narrowband signals) and power of the signal. An example is illustrated in Figure 3.1 for AOA estimation at a uniform linear array (ULA). If the distance between transmitter and receiver nodes becomes sufficiently large, then the incoming signal can be modelled as a planar wave-front and the difference between the arrival times as consecutive array elements becomes ℓ sin ψ/c seconds. ℓ is the inter-element spacing, ψ is the AOA and *c* represents the speed of light, hence the estimation of the time-differences provides angle information. (Gezici, 2008)

For a narrowband signal, time difference can be represented as a phase shift. However, for UWB systems, time-delayed received signals should be considered.

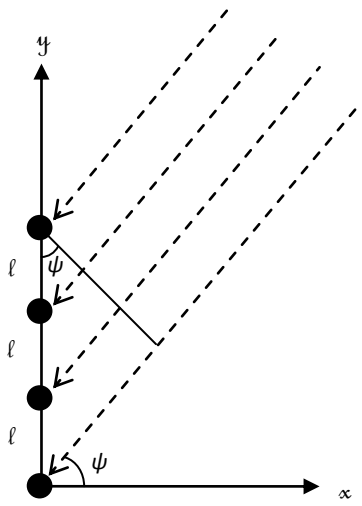

Figure 3.1. Relation between arrival time differences and AOA at ULA.

In order to obtain theoretical lower bounds on the achievable accuracy of AOA measurements, consider a ULA, as shown in Figure 3.2, with N_a antenna elements. Let $r_i(t)$ denote the received signal at the *i*th element, which is expressed as

$$r_i(t) = \propto s(t - \tau_i) + n_i(t), \tag{3.1}$$

for $i = 1, \dots, N_a$, where $s(t)$is the transmitted signal, $\propto$ is the channel coefficient, τ_i is the delay for the signal arriving at the *i*th antenna element, and $n_i(t)$ is white Gaussian noise with zero mean and a spectral density of of $\mathcal{N}_0/2$. (Gezici, 2008)

For independent noise at different antenna elements, CRLB (Cramer-Rao Lower Bound) for estimating ψ is given by

$$\sqrt{\mathrm{Var}\{\hat{\psi}\}} \geq \frac{\sqrt{3}c}{\sqrt{2}\pi\sqrt{\mathrm{SNR}}\,\beta\sqrt{N_a(N_a^2-1)\ell\cos\psi}}, \tag{3.2}$$

where $\mathrm{SNR} = \alpha^2 E/\mathcal{N}_0$, with *E* denoting the energy of the signal $s(t)$, is the signal-to-noise (SNR) ratio for each element, and β is the effective bandwidth. (Mallat, Louveaux and Vandendorpe, 2007)

It is noted from Eq. 3.2 that an increase in the SNR, effective bandwidth, inter-element spacing or the number of antenna elements enhances the accuracy of the AOA estimation. Therefore, the large bandwidth of UWB signals can improve the accuracy of the AOA measurements.

For AOA, the position of the target node can be estimated from two reference nodes by using geometric techniques. This technique solves the position by intersecting two lines and is called as a triangulation (see Fig. 3.2). Let ψ_1 and ψ_2 denote the angles measured by reference node 1 and 2, respectively. Then, the following equations are solved for the position of the target: (Gezici, 2008)

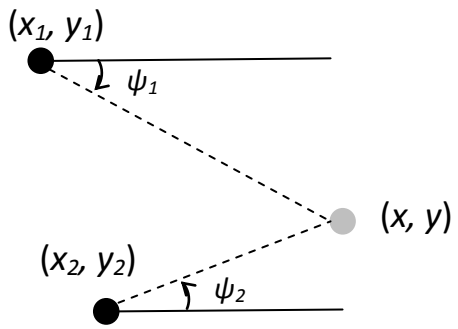

Figure 3.2. Triangulation technique.

$$\tan\psi_1 = \frac{y - y_1}{x - x_1} \qquad \tan\psi_2 = \frac{y - y_2}{x - x_2} \tag{3.3}$$

which yields

$$x = \frac{x_2 \tan\psi_2 - x_1 \tan\psi_1 + y_1 - y_2}{\tan\psi_2 - \tan\psi_1} \tag{3.4}$$

and

$$y = \frac{(x_2 - x_1)\tan\psi_1 \tan\psi_2 + y_1 \tan\psi_2 - y_2 \tan\psi_1}{\tan\psi_2 - \tan\psi_1}. \tag{3.5}$$

3.2. Time of Arrival

Time of arrival (TOA) measurements provide information about the distance between two nodes by estimating the time of flight of a signal that travels from one node to the other. Geometrically, TOA position technique solves the position of the target node as the intersection of position lines obtained from a set of measurements at a number of reference nodes (see Fig. 3.3). This estimation method is called as *trilateration*. The reference (black) nodes measure (with TOA or RSS estimation) their distances from the target node (grey), which results in three circles passing through the black node. The intersection of the three circles can be solved to obtain the position of the target node.

Let d_1, d_2 and d_3 represent the range measurements obtained from three TOA or RSS measurements. Then, the following three equations must be solved jointly in order to estimate the position of the target via trilateration:

$$d_i = \sqrt{(x_i - x)^2 + (y_i - y)^2}, i = 1,2,3, \tag{3.6}$$

where (x_i, y_i) is the known position of the ith reference node, and (x, y) is the position of the target node. The position (x, y) can be solved from Eq. 3.6 as

$$x = \frac{(y_2 - y_1)\gamma_1 + (y_2 - y_3)\gamma_2}{2[(x_2 - x_3)(y_2 - y_1) + (x_1 - x_2)(y_2 - y_3)]}, \tag{3.7}$$

$$y = \frac{(x_2 - x_1)\gamma_1 + (x_2 - x_3)\gamma_2}{2[(x_2 - x_1)(y_2 - y_3) + (x_2 - x_3)(y_1 - y_2)]}, \quad (3.8)$$

where

$$\gamma 1 = x_2^2 - x_3^2 + y_2^2 - y_3^2 + d_3^2 - d_2^2\,, \quad (3.9)$$

$$\gamma 2 = x_1^2 - x_2^2 + y_1^2 - y_2^2 + d_2^2 - d_1^2\,. \quad (3.10)$$

The TOA measurement at a node provides an uncertainty region around a circle as shown in Figure 3.6. To prevent ambiguity in TOA estimates, the two nodes must have a common clock or they must exchange timing information (i.e. synchronised) via certain protocols, such as two-way ranging (TWR) protocol. The conventional TOA estimation technique is performed by means of matched filtering or correlation operations (Turin, 1960). Let the received signal at a node be expressed as

$$r(t) = \alpha s(t - \tau) + n(t) \quad (3.11)$$

where τ represents the time of arrival, α is the channel coefficient, and $n(t)$ is white Gaussian noise with zero mean and a spectral density of $\mathcal{N}_0/2$. Then, a conventional correlator-based scheme searches for the peak of the correlation of $r(t)$ with a shifted version of the template signal $s(t - \tau)$, for various delays $\hat{\tau}$. Similarly, a matched filter scheme, in which the filter is matched to the signal, estimates the instant at which the filter output attains its largest value. These schemes are optimal for single-path AWGN channels.

It should be noted that UWB channels are commonly more complicated than the model assumed in Eq. 3.11.

For the signal model in Eq. 3.11 Cramer–Rao lower bound (CRLB) for estimating the distance can be expressed as

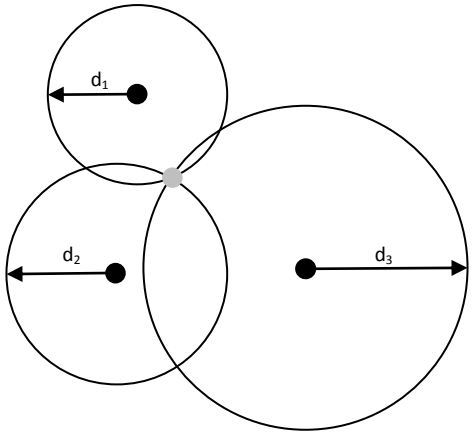

Figure 3.3 The intersection obtained from three TOA (or RSS) estimates, which can be used to solve the position of the target node. This technique is called as *trilateration*.

$$\sqrt{\mathrm{Var}(\hat{\tau})} \geq \frac{1}{2\sqrt{2}\pi\sqrt{\mathrm{SNR}}\beta}, \tag{3.12}$$

where $\hat{\tau}$ represents an unbiased TOA estimate, $\mathrm{SNR} = \alpha^2 \mathrm{E}/\mathcal{N}_0$ is the signal-to-noise ratio, with E denoting the signal energy, and β is the effective signal bandwidth. (Poor, 1994)
Note from Eq. 3.12 that, the accuracy of a TOA measurement can be improved by increasing the SNR and/or the effective signal bandwidth. Since a UWB signal has very large bandwidth, this property allows highly accurate distance estimation using TOA measurements via UWB radios. According to the CRLB bound for various pulse widths, the theoretical limits are of the order of a few centimetres for reasonable SNR values, which indicate the high precision potential of UWB positioning based on TOA measurements.

3.3. Time Difference of Arrival

Conventionally, TOA-based range measurements require synchronization among the target and the reference nodes. However, Time Difference of Arrival (TDOA) measurements can be obtained even in the absence of synchronization between the target node and the reference nodes, if there is synchronisation among the reference nodes (Caffery, 1999). In this case, the difference between arrival times of two signals travelling between the target node and the two reference nodes is estimated. This locates the target node on a hyperbola, with foci at the two reference nodes, as shown in Figure 3.4.

One way to obtain a TDOA measurement is to estimate TOA at each reference node and then to obtain the difference between two estimates. Specifically, if the received signals are given by $\mathrm{r}_1(\mathrm{t})$ and $\mathrm{r}_2(\mathrm{t})$ as in Eq. 3.1, $\tau_1$is estimated from $\mathrm{r}_1(\mathrm{t})$ and τ_2 is estimated from $\mathrm{r}_2(\mathrm{t})$. Since the target node and the reference nodes are not synchronised, the TOA estimates at the reference nodes include a timing offset in addition to the

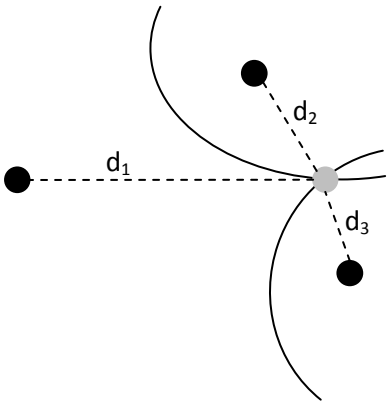

Figure 3.4. TDOA positioning technique.

time of flight. As the reference nodes are synchronised, the timing offset is the same for each TOA estimation. Therefore, the TDOA measurement can be obtained as

$$\hat{\tau}_{TDOA} = \hat{\tau}_1 - \hat{\tau}_2 \,, \tag{3.13}$$

where $\hat{\tau}_1$ and $\hat{\tau}_2$ denote the TOA estimates at the first and second nodes, respectively. Hence it is shown in previous section that the accuracy of TOA measurements increases with bandwidth and SNR, the same conclusions hold true for TDOA measurements when they are estimated from TOA measurements as in Eq. 3.13. (Gezici, 2008)

3.4. Received Signal Strength

Indoor positioning approaches based on communication systems typically use the received signal strength (RSS) as measurements. RSS measurements provide information about the distance between nodes based on some certain channel characteristics. The main idea is that if the relation between distance and power loss is known, the RSS measurement at a node can be used to estimate the distance between that node and the transmitting node, assuming that the transmit power is known.

The distance between two nodes provides a circle of uncertainty for the position of the target node, as shown in Figure 3.5. However, due to inaccuracies in bots RSS measurements and quantification of the distance versus path loss (PL) relation, distance estimates are subject to errors. Therefore, in reality each RSS measurement defines an uncertainty area instead of a circle, such as the one in Figure 3.6.

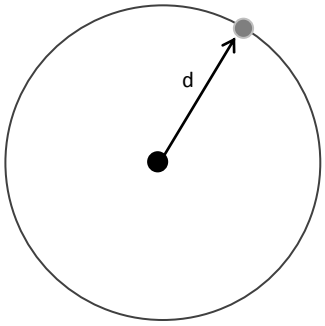

Figure 3.5. The node in the centre measures the RSS and defines a circle around itself with distance *d*.

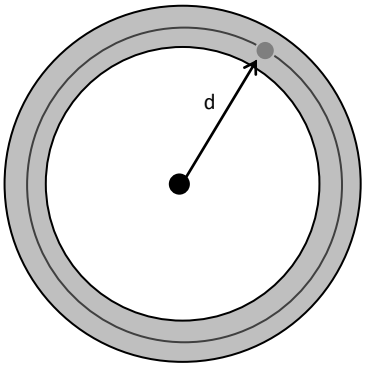

Figure 3.6. The node in centre measures the RSS and determines the distance *d* with some uncertainty.

A UWB signal experiences multipath (small-scale fading), shadowing and path loss while travelling from one node to another. Ideally, average RSS (i.e. power) over a sufficiently long time interval would exclude the effects of multipath fading and shadowing and would result in the following model

$$\bar{P}(d) = P_0 - 10n\log_{10}\left(\frac{d}{d_0}\right), \tag{3.14}$$

where $\bar{P}(d)$ is the average received power in dB at a distance d and P_0 is a constant term representing the received power in dB at a reference distance d_0. The model parameter n is in free space equal with 2. In indoor environments, n typically has a value between 2 and 6.
For the UWB, the multipath effects can be mitigated by measuring the sum of the powers of multipath components. The small-scale fading can be mitigated if the received signal *r(t)* includes all the multipath components in the calculation of the average power over the interval T,

$$P(d) = \frac{1}{T}\int_0^T |r(t)|^2 dt. \tag{3.15}$$

Sometimes there can be shadowing effects present in the received power P(d), which can be modelled as a log-normal random variables, then the received power can be modelled as a Gaussian random variable with mean $\overline{\mathrm{P}}(\mathrm{d})$ (given in Eq.3.14) and variance σ_{sh}^2, in other words

$$10\log_{10} P(d) \sim \mathcal{N}\left(P(d), \sigma_{sh}^2\right). \tag{3.16}$$

This model can be used in both LOS (Line-of-sight) and NLOS (Non line-of-sight) scenarios by using an appropriate channel-related parameter value, e.g. See Table 3.1.

From the received power model in Eq. 3.16, the Cramer-Rao lower bound (CLRB) for distance estimation can be expressed as

$$\sqrt{\mathrm{Var}\{\hat{d}\}} \geq \frac{ln10}{10}\frac{\sigma_{sh}^2}{n}d, \tag{3.17}$$

where $\hat{d}$ represents an unbiased estimation of *d*. It is observed from the equation that since RSS measurements vary more around the true average power, the lower bound increases as the standard deviation of the shadowing increases. Also, a larger path loss exponent results in a better estimation accuracy, as the average power becomes more sensitive to distance for larger n. Finally, the distance dependence structure of Eq. 3.17 indicates that the accuracy of RSS measurements deteriorates as the distance between the nodes increases. (Sahinoglu, Gezici and Güvenc, 2008)

Positioning systems which are based on signal strength have been developed to locate the wireless LAN nodes within buildings. Unfortunately, received signal strength varies not only with distance, but also with composition of the media, through which the signal has propagated (air, concrete, metal, etc.), and the relative orientations of the transmitting and receiving antennas. Some systems are set up to give a simple indication of proximity to other nodes, others use a fixed infrastructure of base stations to provide a positioning capability, but reported accuracy is around 10 m (95%, 2D) (Bahl and Padmanabhan, 2000). Some other systems, such as *Ekahau* positioning system (Ekahau Incorporated, 2010), use standard IEEE 802.11 access points, but require extensive surveys of the building to get enough statistics of the received signal strength indicator (RSSI) to be able to fingerprint the position of the tag to a claimed position accuracy of 1 m.

Table 3.1. Example of channel parameters in difference scenarios

	n	σ_{sh}
Residential LOS	1.79	2.22
Residential NLOS	4.58	3.51
Indoor office LOS	1.63	1.90
Indoor office NLOS	3.07	3.90

4. MEASUREMENTS, ANALYSIS AND RESULTS

In all of our experiments, we used hardware and software procured from Ubisense. The goals were to measure the accuracy of the Ubisense RTLS and test the functionality in various radio environments. Precision/Accuracy Measurements were done in two different environments, in line-of-sight (LOS) deployment and non-line-of-sight (NLOS). Non-line of sight was divided into soft non-line-of-sight (Soft NLOS) and hard non-line-of-sight (Hard NLOS). The idea of the line-of-sight deployment is to test the system in normal indoor conditions while the non line-of-sight deployments are in difficult and challenging conditions.

4.1. Ubisense Sensor Network

Hardware and software procured from Ubisense was used in this thesis. Ubisense RTLS (Real Time Location System) was one of the first commercial companies to utilise the Ultra wideband for real time localisation (Ubisense Ltd., 2010). Ubisense hardware is comprised of two entities: A tag which emits UWB pulses when triggered by the system, and receivers (or Sensors) which are typically fixed devices at the corners of the measurement volume. The Ubisense uses a combination of Time-Difference of Arrival (TDOA) and Angle of Arrival (AOA) techniques to determine the location of a transmitting tag. The company promises a location accuracy of 15 cm in a typical open environment.

The Ubisense platform consists of three main components:

- The RTLS Sensor Network Hardware (Sensors and Tags)
- The LocationEngine (LE) Software, for managing and configuring the hardware
- The Location Platform Software, for data storage and processing

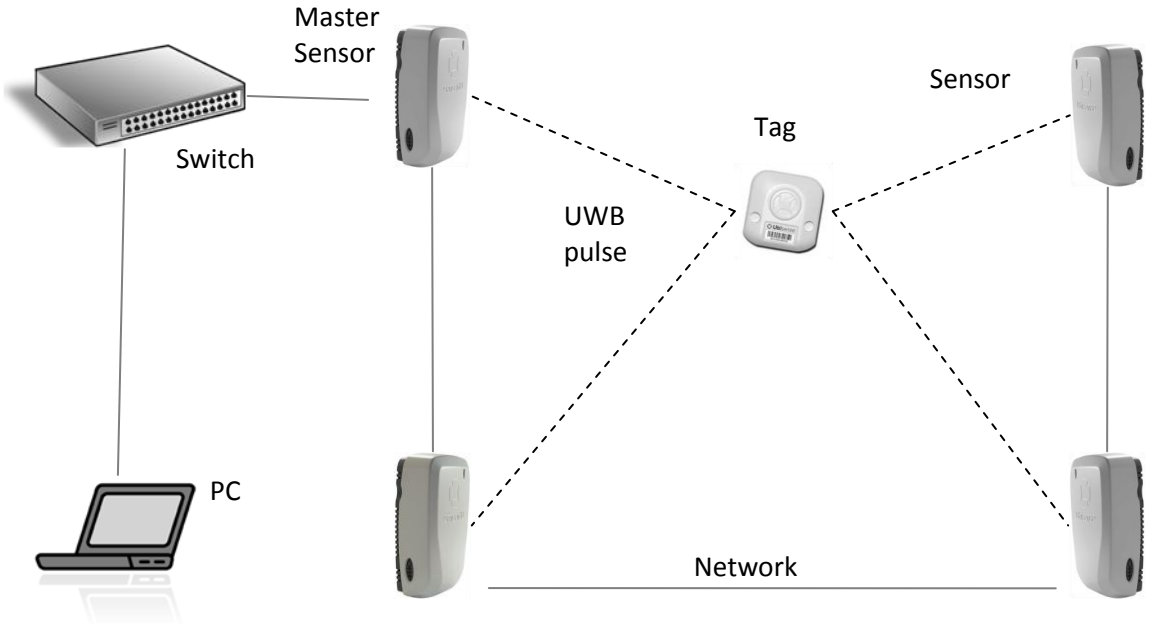

Figure 4.1. The architecture of the Ubisense system. Sensors are networked together, powered by PoE switch and controlled by PC with Location Engine.

4.1.1. RTLS Sensor Network Hardware

The RTLS Sensor Network Hardware consists of the Ubisense Series 7000 sensors and Slim or Compact Tags. The sensors estimate the location of a tag by determining Angle of Arrival (AOA) and Time-Difference of Arrival (TDOA) from the UWB signal of the tag. For TDOA the sensors use Ethernet timing cable as a synchronisation medium. The sensors are organised into cells, typically composed of four to seven sensors, so that each cell covers a defined area. Each cell has one Sensor that functions as its master, which collects and processes the data of the other sensors and generates location events to the LocationEngine over the Ethernet using UDP (User Datagram Protocol). This is called as the Ubisense OTW protocol (On the wire protocol). The master coordinates a TDMA network by using the conventional RF channel (2.4 GHz) by allocating each active tag in the area to an appropriate schedule of slots. The Figure 4.1 shows the architecture of the system. (Ubisense Ltd., 2010)

4.1.2. Sensor Details

The Ubisense series 7000 sensor is approximately 20 cm x 13 cm x 6 cm. It has a ball-and-socket mounting bracket to mount it to the wall and to adjust it in any desired angle. In the middle of the front plane there is a fiducial mark to use for the calibration survey. The backside has six timing cable connections and a network connection. The sensor has a 6 – 8 GHz phased array of UWB receivers for positioning and a bi-directional 2.4 GHz radio communication system for controlling data. The sensor's field of view is about 100 degrees horizontal and 90 degrees vertical with a range of up to 100 meters depending on the radio environment. The antenna array enables detection of Angle of Arrival and timing cable connection enables Time-difference of Arrival. The Sensors can be powered over a network cabling using Power-over-Ethernet (PoE) switches. The Sensors have a boot ROM firmware and with the location engine software the sensors can be remotely configured and monitored. LEDs on the side of the sensors indicate their basic status. (Ubisense Ltd., 2010)

Figure 4.2. Ubisense Series 7000 Sensor. (Ubisense Ltd., 2010)

4.1.3. Ubisense Tag

A Ubisense Tag is a small tag worn by a person (vertical placement) or attached to an object (horizontal placement) allowing it to be accurately located within an indoor environment. The dimensions are approximately 80 mm x 40 mm x 10 mm (Slim tag), 40 mm x 40 mm x 20 mm (Compact tag) and a recently released Ubisense tag module 24.5 mm x 24.5 mm x 9.1 mm. A lithium coin cell battery allows more than 4 years of operating time in a typical application. Tags are equipped with a pair of buttons, two LEDs and a beeper to support control and paging applications. Each tag has a conventional bi-directional RF-transceiver and a UWB transmitter. When the tag is stationary, it goes to sleep state to conserve power, and an in-built motion detector ensures the tag transmits again as soon as it is moved. When the tag is active, it sends out conventional RF packet containing its identity together with a UWB pulse sequence which is used by the Sensors and Location Engine to determine the tag's location. (Ubisense Ltd., 2010)

Figure 4.3. Slim tag (left) and Compact tag (right).
(Ubisense Ltd., 2010)

4.1.4. Location Engine (Location Platform)

Ubisense software package includes several programs. The core program Location Engine (LE) Configuration software can be installed on Windows or Linux operating system. It allows configuring, monitoring and testing the sensors. The LE allows the user to set filter parameters for the tags and configuring and setting the sensors to cells. Automated calibrations are also done in the LE. The software package also includes visualisation tools for improved usability and simulator tool, which allows the user or developer to create simulation scripts describing motion and behaviour of the tracked people and object. The simulator tool is suitable for testing user applications without using the hardware itself. (Ubisense Ltd., 2010)

4.1.5. Developer API

The Ubisense software package includes a fully-featured .NET C# or C++ API for system integration. The API allows user to use a large proportion of settings and data and extends the Location Platform with a Data Dictionary editing tool that allows developers to create new application-specific data models. The APIs are fully open so that integration options are unrestricted: everything that can be done using Ubisense tools can be done via Ubisense API. (Ubisense Ltd., 2010)

4.2. Measurement Concepts

This section covers some essential concepts related to the measurements, such as, definition of the calibration settings, calibration of the system and interpreting the results.

4.2.1. Pitch, yaw, roll and cable offset definitions

The yaw, pitch and roll orientation of each sensor must be determined so that the measured Angle of Arrival can be used to locate tags robustly. The Ubisense uses the aeronautical definitions of yaw, pitch and roll, as shown in Figure 4.4.

The pitch measures the rotation of the sensor along y-axis. It measures how far upward the sensor is pointing, where 0 degrees indicate the sensor is perfectly level, negative numbers mean the sensor is pointing down and positive numbers mean the sensor is pointing up.

The yaw measures the rotation of the sensor along z-axis. It measures the direction the sensor is pointing in, where 0 degrees is pointed along the positive x-axis from the origin and 90 degrees is pointed along the positive y-axis from the origin.

Figure 4.4. Aeronautical orientations. (ZeroOne, 2007)

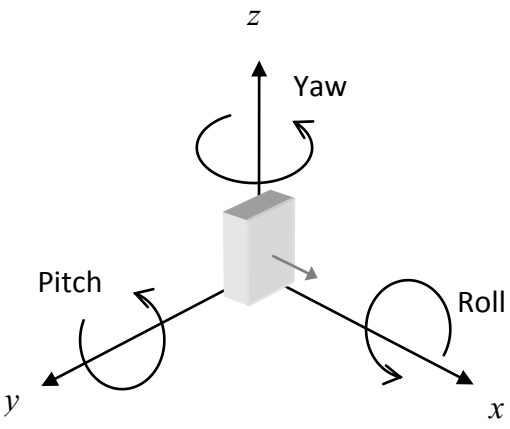

Figure 4.5. Definitions of Yaw, Pitch and Roll along coordinate axes.

The roll measures the rotation of the sensor along x-axis. In the Ubisense this is set to 0 degrees by using a spirit level meter. These previously described orientations are shown in Figure 4.5.

In order to use the TDOA positioning technique in the Ubisense, the sensors require synchronisation between them. Ubisense has implemented the synchronisation via Ethernet timing cables and the length of the timing cable determines the timing delay. This delay must be known precisely for the Ubisense in order to calculate the tag positions. The timing delay, that is, cable offset can be calculated in the LocationEngine. The cable offset is set only to slave sensors.

4.2.2. Geometric dilution of precision

In the deployments the 3D accuracy (XYZ) is usually notably worse than 2D (XY), this is due to the geometry the sensors were deployed. For instance, in a TDOA system with a mobile tag and four receivers as shown in Figure 4.6 where all receivers are equidistant from the transmitter and so all will get the same pseudorange value. However, this condition (that all pseudoranges data are equal) locates at all points along the dashed line and variations in the pseudorange value might be due to changes in the transmitter-receiver distance or variations in the unknown clock offset. Therefore the system will be inaccurate in the Z-dimension with transmitter at X-Y position, because this specific geometry of the transmitters and receivers lead to magnification of ranging errors.

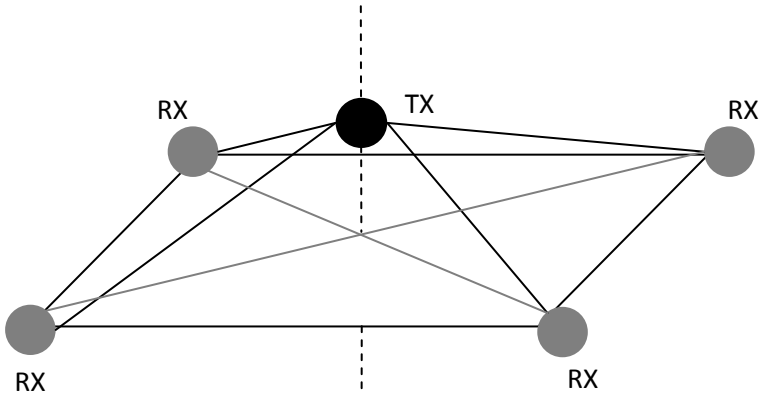

Figure 4.6 Geometric Dilution of Precision in a TDOA system

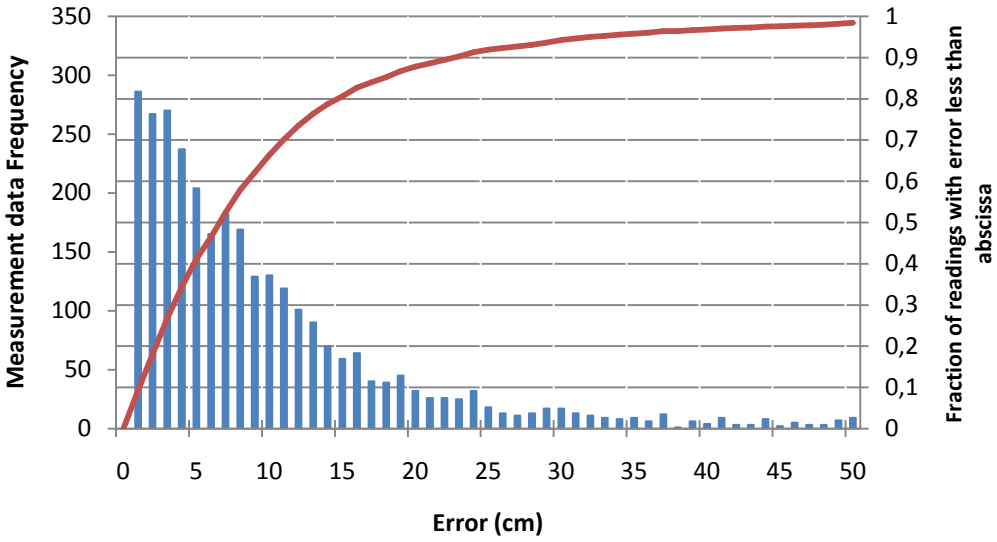

Figure 4.7. A cumulative probability graph along with histogram describing measurement accuracy

4.2.3. Positioning system accuracy analysis

Some developers of location sensor systems often describe their systems as being "accurate to *x* cm", but declarations like this provide only rough information of how a system performs in practice. For instance, it is not likely that the system will always be accurate within that *x* centimetres, as most of the sensor systems generate some amount of noisy outlying readings.

An informative way of describing location system accuracy is by using a cumulative probability graph (also called as, cumulative distribution function, CDF) showing the fraction of readings having an error less than or equal to some value. A typical cumulative probability graph for a UWB location system can be seen in Figure 4.7. For instance, it can be seen that 60 % of the measurement readings produced by the system lie within 10 cm of the true position, and 95 % lie within 35 cm. Comparing data in this graphical form, researchers and designers of different systems can use same graph to determine whether or not the system is suitable for their needs and applications. This method of describing the measurement accuracy is used in this thesis as it is easy and convenient way to present a comparison between measurements and different calibration methods.

4.2.4. System calibration

The calibration of the receivers' position and orientation are crucial in achieving accurate location estimates. The coordinates of a receiver's position was estimated via manual methods by measuring the distance using a tape measure and a laser rangefinder from the receiver centre to a known point in the environment. Accurate estimation of the sensor's orientation (yaw, pitch and roll) is more difficult without special equipment, and additionally there can be some misalignment between the casing of the sensor and the plane of the UWB receiver antenna inside. Therefore it is calibrated electronically.

The Ubisense's proprietary calibration method estimates sensors' pitch, yaw and cable offset. This requires knowing the location co-ordinates (X, Y, Z) of the sensors and a location of a tag in order to compute orientation (yaw and pitch) and cable offset for the sensor. When performing calibration with the Ubisense, the tag was placed as near as possible to the boresight of the calibrated receiver(s). This calibration will be referred in the measurement chapter as Single Point.

The Ubisense's calibration method was utilised to a multi-point measurement by collecting calibration data across the whole measured area for all the sensors. The calibration points which are mostly the same as used in the evaluation cover the whole measured area. To remove poor pitch, yaw and cable offset estimates typically due to poor line-of-sight or environmental reflections, median filtering was used. This calibration will be referred in the measurement chapter as Multi-point Median.

The Ubisense also has an automatic calibration mode in the LocationEngine. In the automatic mode, a tag is placed at several locations within the measurement volume where the height of the tag is known and provided by the user to the LocationEngine. The system takes measurements to estimate the X and Y position of the tag and the pitch and yaw of calibrated receivers. However, this calibration method failed in all of the deployments and therefore it was not possible take it into account for the comparisons.

4.3. Deployments

Approximately 100 raw position estimates per measurement point were collected in every deployment. Readings were taken with a stationary compact tag placed at a height of 0.91 cm above the floor. The positions of the sensors and the measurement points were manually surveyed using tape measure and laser rangefinder. In Line-of-sight (LOS) deployment the sensors and points were surveyed with accuracy of ±2 cm and in Non line-of-sight (NLOS) deployments with ±5 cm accuracy.

4.3.1. Line-of-Sight

In line-of-sight (LOS) deployment four sensors (receivers) were deployed covering an area of approximately 3 x 7 m into a relatively empty room, with some chairs and desks along the wall of the room (see Fig. 4.8). The idea of this deployment was to test the system in a typical office space containing office furniture and some metallic objects.

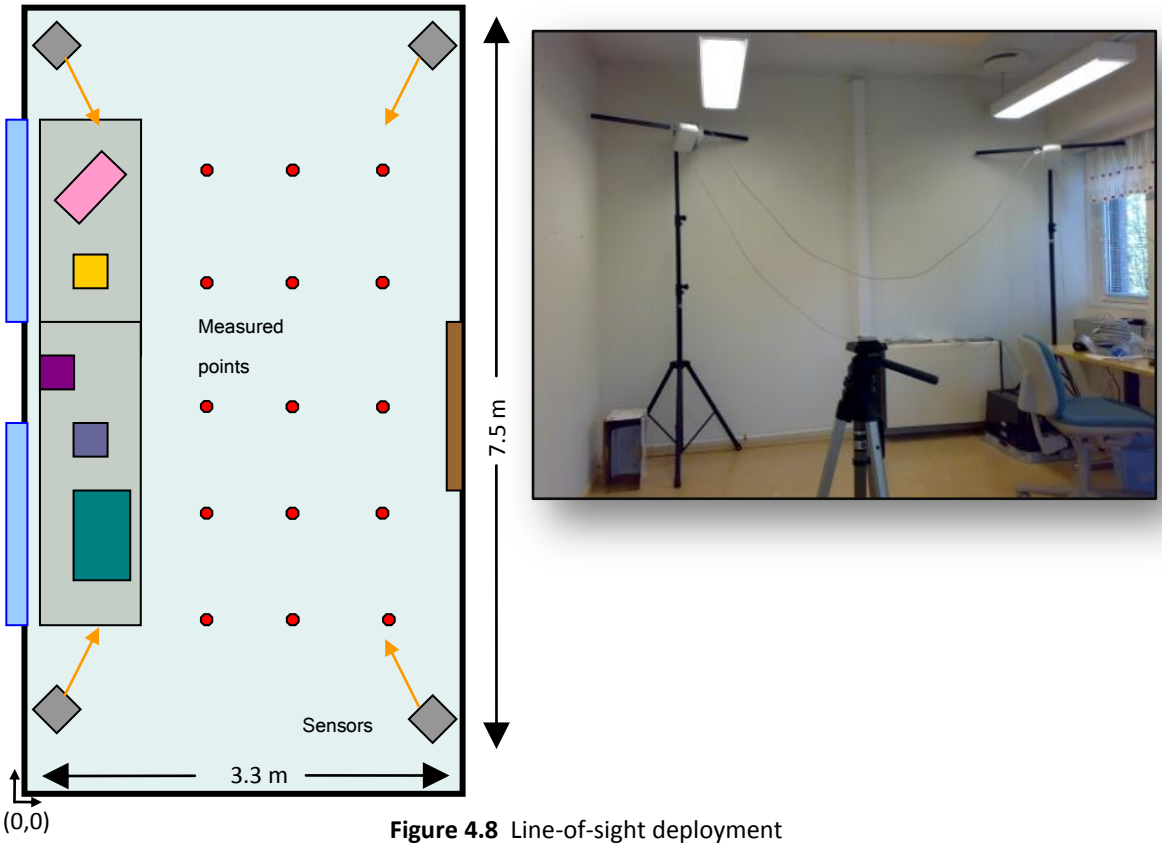

Figure 4.8 Line-of-sight deployment

15 test-points were arbitrarily chosen across the measurement area. 100 data samples per measurement point were collected for the cumulative comparison figures (Fig. 4.9). The sensors' calibration with the Single point calibration was done at the central point of the measurement area and multi-point median calibration was done from all the 15 measurement points. Table 4.1 shows the values acquired from single and multi-point median calibrations.

Table 4.1. Calibration settings used in line-of-sight measurements

Single point	*Sensor 1*	*Sensor 2*	*Sensor 3*	*Sensor 4*
Pitch (deg)	-26.4	-25.1	-27.9	-23.9
Yaw (deg)	-28.9	27	-148.6	161.3
Cable offset		1429.9	332.7	338.9
Multi-point Median calibration				
Pitch (deg)	-27.8	-25.8	-28.6	-23.9
Yaw (deg)	-29	28.6	-149.7	161.7
Cable offset		1425.8	329.6	336.2

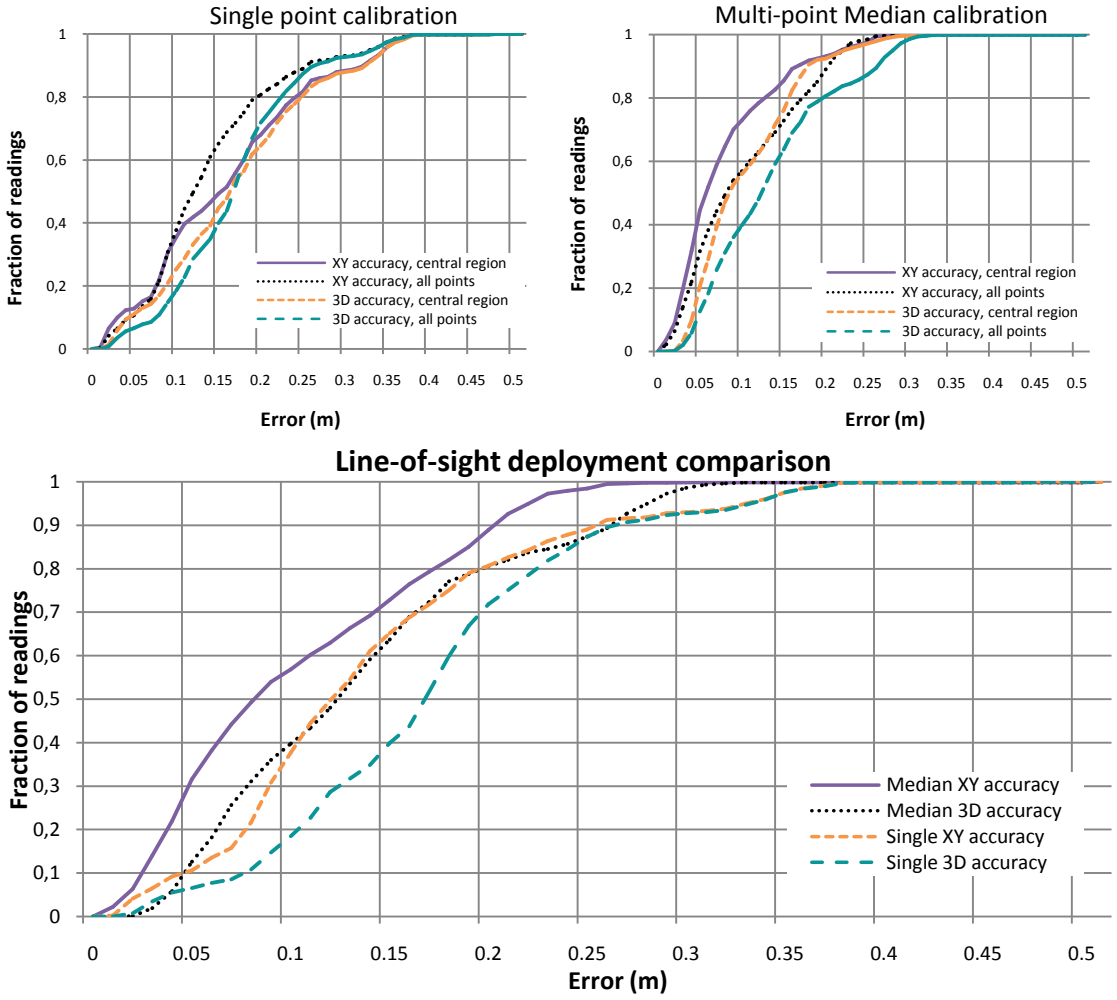

Figure 4.9. Cumulative distribution functions describing the results of the Line-of-sight measurement.

When using the Single-point calibration in the Line-of-sight deployment, Ubisense achieved ca. 27 cm accuracy both in XY and 3D at 90 % precision. When utilising Multi-point median calibration the system achieved ca. 20 cm in XY and 27 cm in 3D at 90 % precision.

The Single-point calibration figure shows that the system performed better when all the measurement points were included. It seems that the central measurement area caused measurement errors which might have caused by an inaccurate calibration.

4.3.2. Soft Non Line-of-Sight

Positioning systems are often demonstrated in environments where line of sight is guaranteed, but usually interesting applications for UWB as an asset tracking system will need to be able to handle much more challenging conditions and multipath components. Severe multipath makes in fact the process of estimating the direction and the time of flight extremely difficult and its effects need to be removed.

The Soft Non Line-of-Sight (Soft NLOS) deployment was set-up in a factory-like environment where large amount of metallic objects exist. In this deployment, some measurement points were chosen so that there is a line-of-sight only to one sensor and the direct signal path lightly obstructed to others.

17 measurement points were used across the covered measurement area of 10 x 7 m. The sensors at the right side were at a height of about 3.4 meters and the sensors on the left side at a height of around 2.4 m. The environment contains a large amount of metallic objects and items. The set-up is shown in the Figure 4.10.

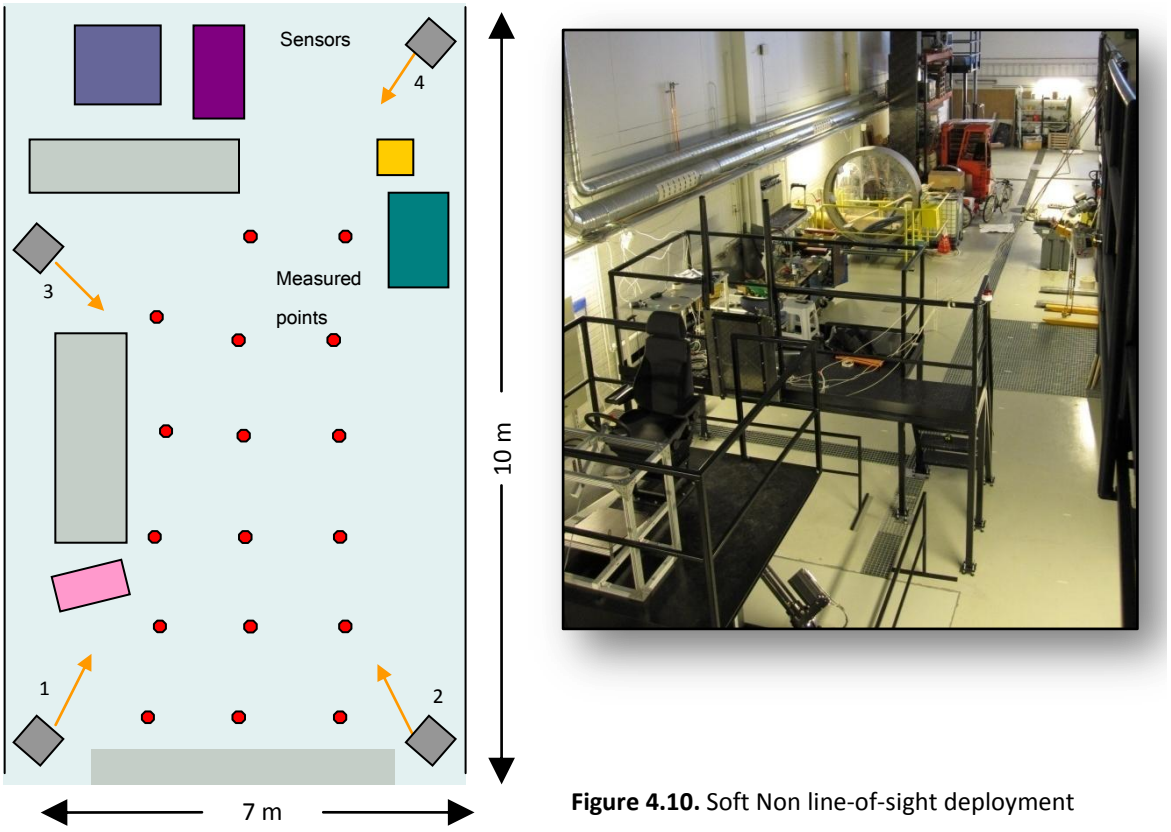

Figure 4.10. Soft Non line-of-sight deployment

Table 4.2. Calibration settings used in Soft Non line-of-sight measurements

Single point calibration	*Sensor 1*	*Sensor 2*	*Sensor 3*	*Sensor 4*
Pitch (deg)	-22.4	-26.9	-23.2	-26.5
Yaw (deg)	42.1	116.9	-40.6	-116
Cable offset		334.7	332.8	1426.2
Multi-point Median calibration				
Pitch (deg)	-21.1	-27.5	-22.2	-29.1
Yaw (deg)	43.5	115.4	-40.6	-116.8
Cable offset		335	332.2	1426

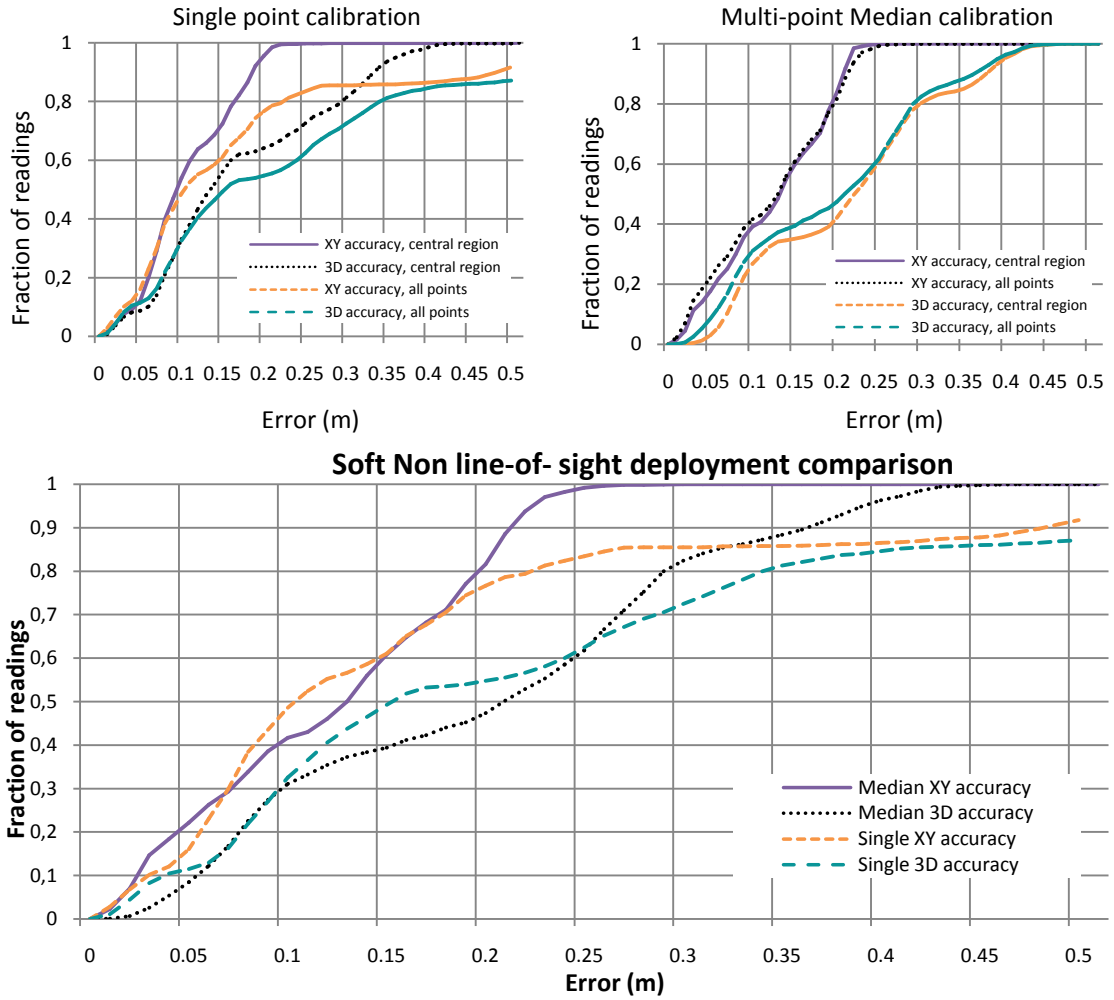

Figure 4.11. Cumulative distribution functions describing the results of the Soft Non line-of-sight measurement

The Figure 4.11 shows the performance of the Ubisense system in the Soft NLOS deployment. From the CDF it can be seen that in Single calibration the system achieved an accuracy of ca. 50 (XY) cm but with 3D it is worse than 50 cm at 90 % precision. In the Median calibration measurement the system achieved an accuracy of ca. 22 cm (XY) and ca. 36 cm (3D) at 90 % precision.

In Median measurement larger measurement area (i.e. outer measurement points included) did not seem to deteriorate the overall accuracy of the system

4.3.3. Hard Non Line-of-Sight

The deployment for Hard NLOS was modified from the Soft NLOS deployment so that the sensors number two and three were moved a bit further away from the central region to create a more hostile environment for the system (see Fig 4.12). Five more points were also added and the locations were chosen so that they were situated in of almost total absence of any penetration in a direct path to most of the sensors. In this deployment a total of 22 measurement points were used and most of the points are situated so that the direct signal path is obstructed by metallic objects to at least two of the sensors.

The harsh radio environment caused the system to generate multiple different calibration parameters. Three different single point calibration parameters along with multi point median were used and the performance results are displayed in Figure 4.13.

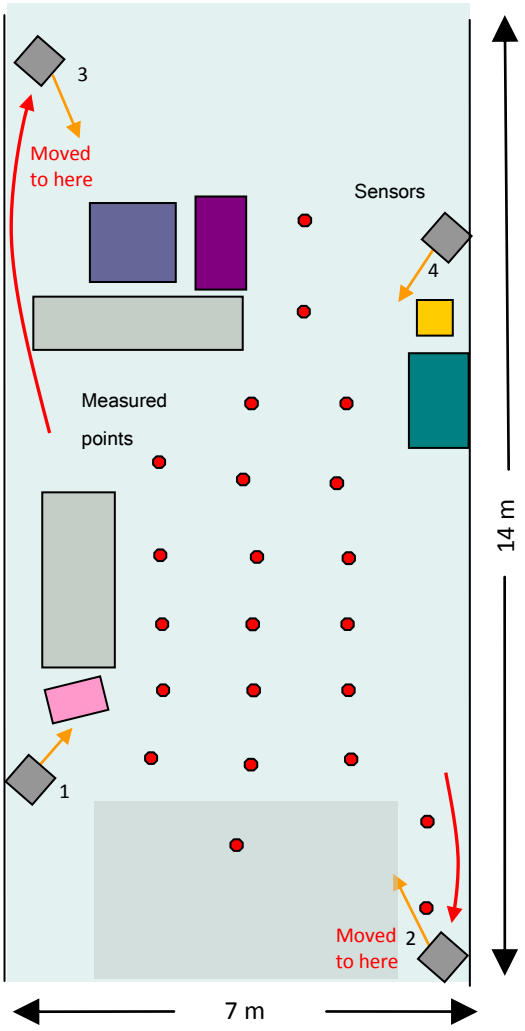

Figure 4.12. Hard Non line-of-sight deployment

Table 4.3. Calibration settings used in Hard Non line-of-sight measurements

Single point calibration	*Sensor 1*	*Sensor 2*	*Sensor 3*	*Sensor 4*
Pitch (deg)	-20.8	-19.4	-9	-29.7
Yaw (deg)	50.5	110.2	-65.7	-118.4
Cable offset		336.7	333.9	1425.9
Multi-point Median calibration				
Pitch (deg)	-21.1	-19.4	-12.3	-29.1
Yaw (deg)	49.7	105	-66.3	-116.9
Cable offset		336.2	332.5	1426.2

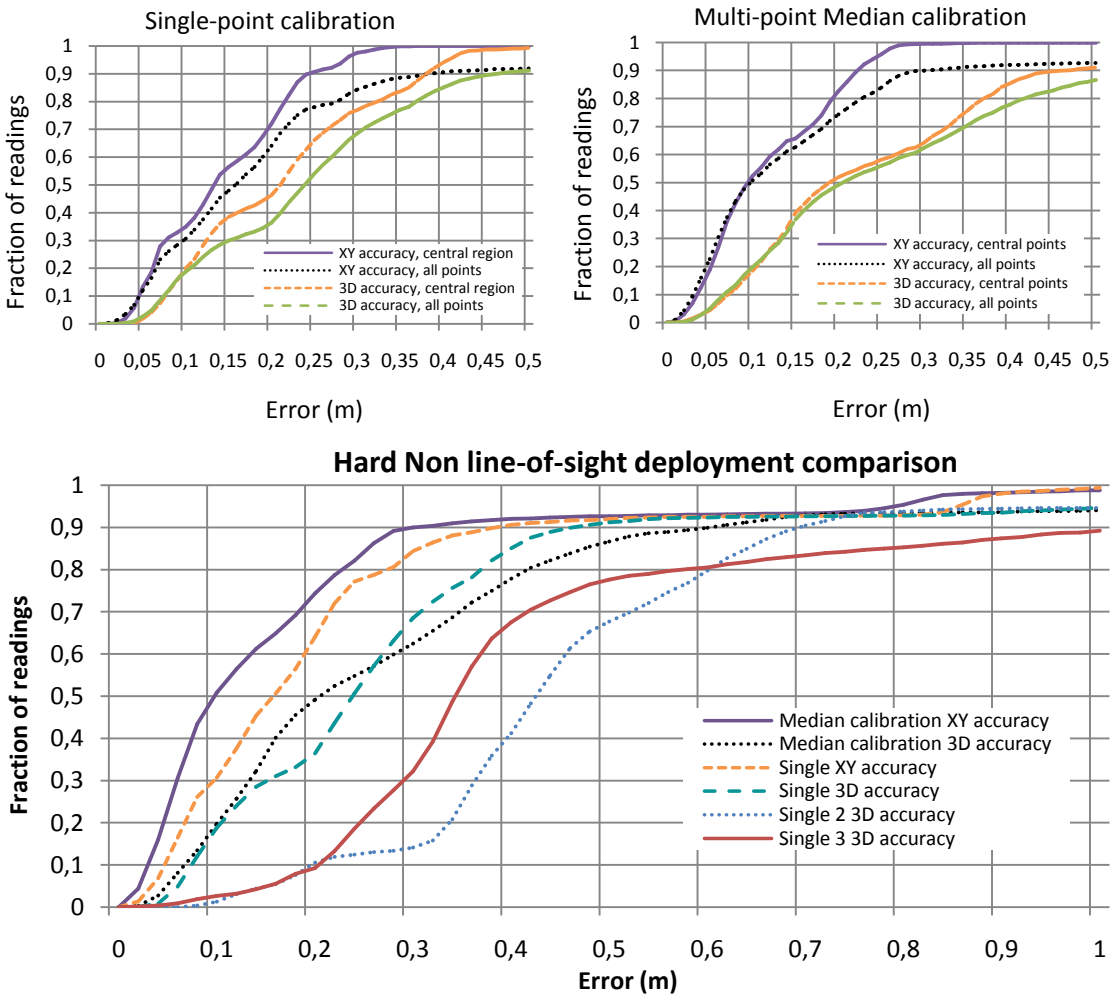

Figure 4.13. Cumulative distribution functions describing the results of the Hard Non line-of-sight measurement

With the best of the Single calibrations the system achieved an accuracy level of ca. 40 cm (XY) and ca. 50 cm (3D) at 90 % precision. When utilising the Multi-point Median, the system achieved ca. 30 cm (XY) and ca. 60 cm (3D) at 90 % precision. In this deployment when using the system with Median calibration parameters the 3D accuracy seemed to be slightly worse than with single calibration parameters.

In the CDF chart most of the readings are under 50 cm, but due to some difficultly located measurement points, residuals of more than one meter appear. Most of the large residual readings were faulty measurements (i.e. the system could not make an estimate), faulty measurements were not removed and in fact they were marked as a penalty (high error, >1m).

This was due to the comparison manner of these calibration methods. In normal conditions position estimates of over 1 m should be able to filter out.

By removing large residuals (over 1 m errors) from the CDF readings, the performance improves and the XY accuracy for Single is 36 cm and 26 cm for Median, 3D accuracy for Single is 40 cm and 46 cm for Median at 90 % precision.

4.4. Conclusion

In general, there are three sources of raw measurement error in any location system: Sensor inaccuracy, calibration inaccuracy (sensor position and orientation) and inaccuracies induced by environmental effects (noise, attenuation and/or reflections).

The Ubisense RTLS positioning system is sensitive to calibration parameters and the Multi-point Median calibration improved the final accuracy of the system in most of the deployments. This kind of calibration method can be easily implemented by calibrating the system using simultaneously multiple tags to collect the calibration data to the database. It increases the installation labour by some amount but could be easily done using a Total Station.

Table 4.4 summarises the positioning accuracy results of the system in the deployments. The Ubisense RTLS performs well in environment where severe multipath exists. This kind of accuracy is enough for many indoor applications where the tracked object is need to be located with proximate location, for instance, in what part of the room object is in.

Table 4.4. Position estimation error (in cm) in the deployments at 95 % confidence level

	Single		*Median*	
	XY	3D	XY	3D
LOS	27	27	20	27
Soft NLOS	50	>50	22	36
Hard NLOS	40	50	30	60

It should be noted that raw location events were used in this study and the system performance can be greatly improved by applying filters and adjusting position estimate algorithm parameters. Another crucial concept affecting the final accuracy is the cell planning. In the NLOS deployments the sensors were deployed in worst-case scenario manner.

5. CALIBRATION OF POSITIONING SYSTEMS

This chapter considers calibration techniques for pseudoranging (or TDOA) and Angle of Arrival based systems. The calibration of the base stations' position and orientation are crucial in achieving accurate location estimates. The xyz-coordinates of a receiver's position can be estimated with sufficient accuracy via manual methods, such as measuring the distance (using a tape measure or laser rangefinder) from the receiver centre to several known points in the environment but can be laborious in large deployments.

There are two different infrastructure systems, active and passive. Here we consider an infrastructure of fixed receiver nodes which listen to a transmitting mobile node (called as an active system). The other one is a passive system which reverses the arrangement so that the fixed nodes transmit while the mobile node listens.

This thesis contributes an algorithm for flexible calibration for base stations basing on Angle of Arrival measurements, evaluates the effectiveness of this algorithm both in simulation and in practice. Also study of AOA data obtained from the sensors, pre-processing and pre-filtering the raw data to get better and more robust estimates.

5.1. Pseudoranging Calibration

Time model based auto-calibration methods have been presented in the work by Duff and Muller for TDOA and TOA estimation techniques (Duff and Muller, 2003). Here the procedure to calibrate a TDOA based system is presented. In pseudoranging system there is no synchronisation signal between the fixed receivers and the mobile transmitter for the transmission timing information. The mobile node transmits a signal at time 0 while the fixed nodes listen for the incoming signals. When the nearest receiver detects the signal at time t_z, a timer is started to measure the relative time difference of arrival t_i as the signal reaches the other *N* receivers at time $t_z + t_i$ $(0 \leq i \leq N)$. Therefore $t_i = 0$ for the nearest receiver, and $t_i \geq 0$ for all other receivers. We indicate the nearest receiver as *zero receiver* F_z. Since the only observable data is the relative arrival time difference t_i, distance measurements cannot be made directly by multiplying with the speed of the signal *c* (that is, the speed of the light in RF-systems). Instead, the unknown time of flight t_z to the zero receiver F_z must first be computed. Then the overall distance between the mobile node and each fixed node is given by $d_i = c(t_z + t_i)$ $(0 \leq i \leq N)$. This is shown as a diagram in Figure 5.1

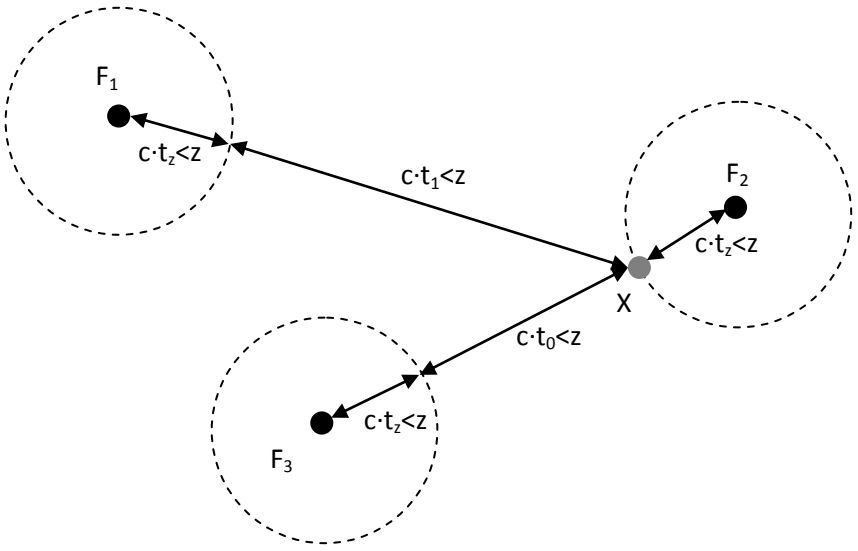

Figure 5.1. Diagram of pseudoranging positioning system. X is the transmitting mobile node., $F_{1..3}$ are the fixed receivers. F_2 is the zero receiver, ie. $\mathbf{c} \cdot \mathbf{t_2} = \mathbf{0}$

Indicating the unknown offset to the zero receiver at mobile node position *j* as $r_{zj} = \mathrm{c} \cdot \mathrm{t}_{\mathbf{z_j}}$ the calibration problem for pseudoranging system is to compute *N* fixed node positions $\mathbf{F_i}$ and *M* mobile node positions $\mathbf{X_j}$ by solving the system of equations given in Eq. 5.1

$$r_{ij} + r_{zj} = \left|\mathbf{F_i} - \mathbf{X_j}\right| \qquad (0 \le i < N, 0 \le j < M) \qquad (5.1)$$

By observing for zero receiver $\mathbf{F_{z_j}}$, the relative distance is $r_{ij} = 0$, we obtain Eq. 5.2. The r_{zj} can be substituted into the other equations to eliminate the offset r_{zj} from the system. This yields a system of $M(N-1)$ equations, shown in Eq. 5.3.

$$r_{zj} = \left|\mathbf{F_i} - \mathbf{X_j}\right| \qquad (5.2)$$

$$r_{ij} = \left|\mathbf{F_i} - \mathbf{X_j}\right| - \left|\mathbf{F_{z_j}} - \mathbf{X_j}\right| \qquad \left(0 \le i < N, 0 \le j < M, i \ne z_j\right) \qquad (5.3)$$

The Eq. 5.3 can now be expressed as a least square minimisation function *F* by summing squared residuals. The minimisation function is shown in Eq. 5.4 where r_{ij} are the observed relative time difference measurements in distances, $\mathbf{F_i}$ are the unknown fixed node positions and $\mathbf{X_j}$ are the unknown mobile node positions.

$$F = \sum_{i=0, i \ne z_j}^{N-1} \sum_{j=0}^{M-1} \left(r_{ij} - \left|\mathbf{F_i} - \mathbf{X_j}\right| + \left|\mathbf{F_{z_j}} - \mathbf{X_j}\right|\right)^2 \qquad (5.4)$$

This method has been applied into ultrasonic positioning system whereby using the auto-calibration a final accuracy of 4 cm at 95 % precision was achieved as compared to manually calibrated system (2.7 cm at 95 % precision). (Duff, 2008)

However, even though Ubisense uses pseudoranging (or TDOA) due to the internal access restrictions it was not possible to study the usability of this method in the UWB.

5.2. Calibration Based on Angle of Arrival

In the Ubisense system, each sensor has six degrees of freedom in space: x_s, y_s, z_s, a_s, b_s and r_s. Where x_s, y_s and z_s are 3D location coordinates, a_s, b_s and r_s are yaw, pitch and roll angles, respectively. Normally in the Ubisense system $r_s = 0$, which is balanced with spirit level. Tags have x_t, y_t and z_t locations and no orientation. Each sensor's parameters (x_s, y_s, z_s, a_s and b_s) define its own frame of reference. In Figure 5.2 the position of the tag in the sensor's frame of reference determines the Angle of Arrival (azimuth *α* and elevation *β).*

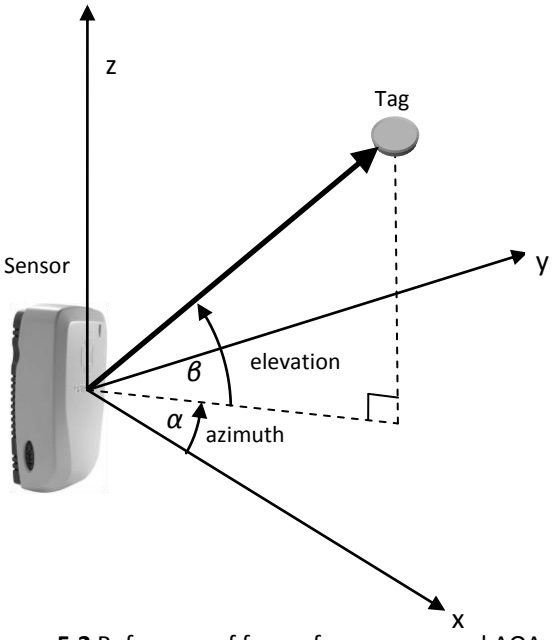

Figure 5.2 Reference of frame for a sensor and AOA of a tag

Each tag/sensor pair introduces two equations. Let x_t^s, y_t^s and z_t^s be the location coordinates of a tag in the sensor's frame of reference and *α* and *β* the azimuth and elevation angles, respectively. From these, the following two equations can be deduced:

$$\begin{cases} x_t^s \sin(\alpha) - y_t^s \cos(\alpha) = 0 \\ x_t^s \sin(\beta) - z_t^s \cos(\beta)\cos(\alpha) = 0 \end{cases} \tag{5.5}$$

where x_t^s, y_t^s and z_t^s can be obtained by the given position of the sensor x_s, y_s, z_s, a_s and b_s and the position of the tag x_t, $y_t$and z_t in a global frame of reference (Zhang, Partridge and Reich, 2007)

$$\begin{pmatrix} x_t^s \\ y_t^s \\ z_t^s \\ 1 \end{pmatrix} = \begin{bmatrix} \cos(a_s)\cos(b_s) & -\sin(a_s) & \cos(a_s)\sin(b_s) & x_s \\ \sin(a_s)\cos(b_s) & \cos(a_s) & \sin(a_s)\sin(b_s) & y_s \\ -\sin(b_s) & 0 & \cos(b_s) & z_s \\ 0 & 0 & 0 & 1 \end{bmatrix} \begin{pmatrix} x_t \\ y_t \\ z_t \\ 1 \end{pmatrix}. \tag{5.6}$$

By using the Eq. 5.5 and Eq. 5.6, the location of the tag (x_t, y_t and z_t) can be solved from given AOA data of two sensors with known locations (four equations, three unknowns). Or a sensor's orientation solved from a fixed tag at known position relative to the sensor (two equations, two unknowns). The Ubisense's proprietary calibration procedure utilises one known sensor position and one known tag position to calculate the orientation parameters for the sensor.

Our work contributes an alternative solution to calibrate the system basing on pin-hole camera model. The calibration based on Angle of Arrival bases on camera calibration technique and eliminates the need to accurately know the positions of the sensors. There are various camera calibration techniques available (Remondino and Fracer, 2006), for both external and internal camera parameters. Generally external parameters comprehend location and orientation in the workspace. Internal parameters comprehend focal length and parameters for radial and decentring distortions.

5.2.1. Pin-hole Camera Model

The pin-hole camera model is used in this algorithm to map Angle of Arrival angular data into positions at an image plane. One of the most used camera calibration techniques is the one proposed by Tsai (Tsai, 1986). The Tsai model is based on a pinhole perspective projection model and is applied to the Ubisense RTLS sensor calibration. The objective is to find out external parameters (position and orientation relatively to a world co-ordinate system). As Illustrated in Figure 5.3, the origin of the camera-centred co-ordinate system (x_c, y_c, z_c) coincides with front nodal point of the camera and the y_c axis coincides with the camera's optical axis. The image plane is assumed to be parallel to the (z_c, x_c) plane at a distance f from the origin, where f is the effective focal length of the camera.

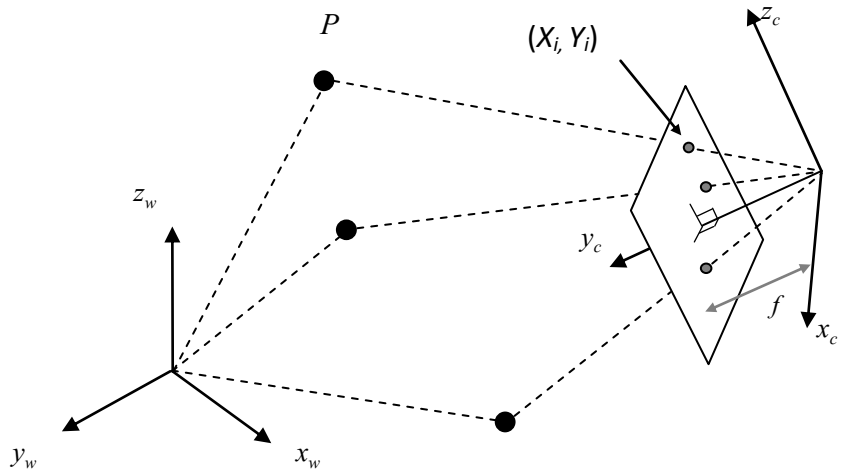

Figure 5.3 Camera model geometry

The relationship between the position of a point P in world co-ordinates (x_w, y_w, z_w) and the point in the camera's image plane (X_i, Y_i) is defined by coordinate transformations. Firstly, a rigid body transformation from the world coordinate system (x_w, y_w, z_w) to the camera-centred coordinate system (x_c, y_c, z_c). This is expressed as

$$\begin{bmatrix} x_c \\ y_c \\ z_c \end{bmatrix} = R \begin{bmatrix} x_w \\ y_w \\ z_w \end{bmatrix} + \begin{bmatrix} T_x \\ T_y \\ T_z \end{bmatrix}, \tag{5.7}$$

where

$$R = \begin{bmatrix} r_1 & r_2 & r_3 \\ r_4 & r_5 & r_6 \\ r_7 & r_8 & r_9 \end{bmatrix} \tag{5.8}$$

is the $3\ x\ 3$ rotation matrix describing the orientation of the camera in the world co-ordinate system. The second transformation is a perspective projection using an ideal pinhole camera model of the point in camera co-ordinates to the position of its image in image plane co-ordinates, (X_i, Y_i). This is described by

$$X_i = f\left(\frac{x_c}{z_c}\right) \tag{5.9}$$

$$Y_i = f\left(\frac{y_c}{z_c}\right). \tag{5.10}$$

5.2.2. Estimation Algorithm

Camera calibration method by Heikkilä (Heikkila et al., 2002; Heikkilä, Koskinen, Lehikoinen 2010) was implemented with the simplifications that no focal length is calculated and pure least squares estimation is applied.

We have the following parameters giving the estimated base station location and orientation in the work space, i.e., its pose $\bar{S}$:

$$\bar{S} = [\alpha \quad \beta \quad \theta \quad x \quad y \quad z]^T \tag{5.11}$$

where *x, y,* and *z* determine the location of the base station in the workspace and θ, β and α determine the rotation of the base station around z, y and x axis in the workspace.

The basic principle of the calibration algorithm is as follows. We locate the measured tag to a known set of calibration points in the work space and measure the corresponding points as Angle of Arrival values of the base station. Then we transform the Angle of Arrival values to a pin hole camera model. After this we compute the pose parameters of the base station so that the errors in the known and measured image plane locations (in x and y directions) of the calibration points are minimised. This is done by using an error function, which determines the deviation of the expected locations of the measured tag point in the “images” compared to the real, measured ones. The error function is non-linear, and we apply the Newton's method for stepwise iteration. This has the origin in the work of Lowe (Lowe, 1985). He found out, that the partial derivatives of the rotational parameters can be represented very simply by the translation parameters, and also that better convergence can be found if the parameter increments are added to the nominal values by a corresponding incremental homogeneous transformation. The equations for the algorithm are given below.

Let the rotations around specific axis and translation be as:

$$\bar{H}_{rot,z} = \begin{bmatrix} \cos(\theta) & -\sin(\theta) & 0 & 0 \\ \sin(\theta) & \cos(\theta) & 0 & 0 \\ 0 & 0 & 1 & 0 \\ 0 & 0 & 0 & 1 \end{bmatrix} \tag{5.12}$$

$$\bar{H}_{rot,y} = \begin{bmatrix} \cos(\beta) & 0 & \sin(\beta) & 0 \\ 0 & 1 & 0 & 0 \\ -\sin(\beta) & 0 & \cos(\beta) & 0 \\ 0 & 0 & 0 & 1 \end{bmatrix} \tag{5.13}$$

$$\bar{H}_{rot,x} = \begin{bmatrix} 1 & 0 & 0 & 0 \\ 0 & \cos(\alpha) & -\sin(\alpha) & 0 \\ 0 & \sin(\alpha) & \cos(\alpha) & 0 \\ 0 & 0 & 0 & 1 \end{bmatrix} \tag{5.14}$$

$$\bar{H}_{trans} = \begin{bmatrix} 1 & 0 & 0 & x \\ 0 & 1 & 0 & y \\ 0 & 0 & 1 & z \\ 0 & 0 & 0 & 1 \end{bmatrix} \tag{5.15}$$

The pose of the base station $\bar{H}_{sensor}$ is presented as a homogeneous matrix in zyx Euler form

$$\bar{H}_{sensor} = \bar{H}_{trans} \times \bar{H}_{rot,z} \times \bar{H}_{rot,y} \times \bar{H}_{rot,x} \tag{5.16}$$

The points in the world frame of reference are converted to the sensor frame of reference by multiplying with matrix

$$\bar{p}_s = \bar{H}_{sensor}{}^{-1} \times \bar{p}_w \tag{5.17}$$

where $\bar{p}_w$ is the point in the global reference frame and $\bar{p}_s$ is the point in the sensor reference frame.

Then the perspective projection maps the 3D points in the base station coordinates into the image plane as

$$\bar{p}_{im} = \begin{bmatrix} p_{im,x} \\ p_{im,y} \end{bmatrix} = \begin{bmatrix} f\dfrac{p_{s,x}}{p_{s,y}} \\ f\dfrac{p_{s,z}}{p_{s,y}} \end{bmatrix} \tag{5.18}$$

The base station pose parameters are estimated by fitting the nominal (predicted) calibration points to the measured calibration points in the image plane. The error between the nominal points and measured (real) points $\bar{dy}$ is then

$$\bar{e} = \bar{p}_{im,nom} - \bar{p}_{im,sensor} \tag{5.19}$$

where $\bar{p}_{im,nom}$ is the expected point location in the plane and $\bar{p}_{im,sensor}$ is the measured Angle of Arrival point location in the image plane.

To calculate correction increments to the base station pose parameters the error function needs to be linearised. This can be done by decomposing the partial derivatives as, that is, the Jacobian

$$J = \frac{\partial \bar{e}}{\partial \bar{S}} = \frac{\partial \bar{e}}{\partial \bar{p}_s} \times \frac{\partial \bar{p}_s}{\partial \bar{p}_w} \times \frac{\partial \bar{p}_w}{\partial \bar{S}} \tag{5.20}$$

where

$$\frac{\partial \bar{e}}{\partial \bar{p}_s} = \begin{bmatrix} \frac{f}{p_{s,y}} & -f\frac{p_{s,x}}{{p_{s,y}}^2} & 0 \\ 0 & -f\frac{p_{s,z}}{{p_{s,y}}^2} & \frac{f}{p_{s,y}} \end{bmatrix}, \tag{5.21}$$

$$\frac{\partial \bar{p}_s}{\partial \bar{p}_w} = R_{sensor} \tag{5.22}$$

and

$$\frac{\partial \bar{p}_w}{\partial \bar{S}} = \begin{bmatrix} 0 & p_{w,z} & -p_{w,y} & 1 & 0 & 0 \\ -p_{w,z} & 0 & p_{w,x} & 0 & 1 & 0 \\ p_{w,y} & -p_{w,x} & 0 & 0 & 0 & 1 \end{bmatrix}. \tag{5.23}$$

One sample, that is, one point measurement gives one row into the Jacobian, one for x error and one for y error. At least 3 samples are needed to estimate the 6 parameters, and more parameters improve the accuracy in a LSQ (Least Squares Qudaratic) sense. The correction increments for the pose parameters are derived as

$$d\bar{S} = [d\alpha \quad d\beta \quad d\theta \quad dx \quad dy \quad dz]^T = -V \times S^{-1} \times U^T \times \bar{e} \tag{5.24}$$

where *U*, *S* and *V* are taken from the singular value decomposition of the Jacobian:

$$[U \quad S \quad V] = \mathrm{svd}(J) \tag{5.25}$$

The estimation procedure goes iteratively. First initial values for the pose parameters $\bar{S}_0 = [\alpha_0 \quad \beta_0 \quad \theta_0 \quad x_0 \quad y_0 \quad z_0]^T$ have to be set. Then the base station pose parameters will be calculated by estimating the increments $d\bar{S}$ and adding these to the initial values

$$\bar{S}_{i+1} = \bar{S}_i + d\bar{S} \tag{5.26}$$

Repeating this iteratively until the increments $d\bar{S}$ are close to zero the final pose parameters will be reached. Typically this takes no more than 6 to 8 steps.

5.2.3. Simulation Results

The performance of the calibration algorithm with regards to measurement noise was studied in a scenario comparable to our test environment. A total of 15 calibration points were used in an area of 11 x 5 m, where the points were separated by one meter and the base station was located in a corner. Figure 5.4 shows the 3D view of the simulated locations of the 15 calibration points and the sensor. The dimensions are in mm.

A Matlab simulator was developed to simulate the data given by the Ubisense and to find out how the algorithm behaves by using different size and form of calibration pattern. The simulated Angle of -Arrival data was generated from the calibration points by converting from Cartesian coordinates (xyz) to azimuth ($\propto$) and elevation (β) angles (see Fig. 5.5). This was done by Eq. 5.27 and Eq. 5.28

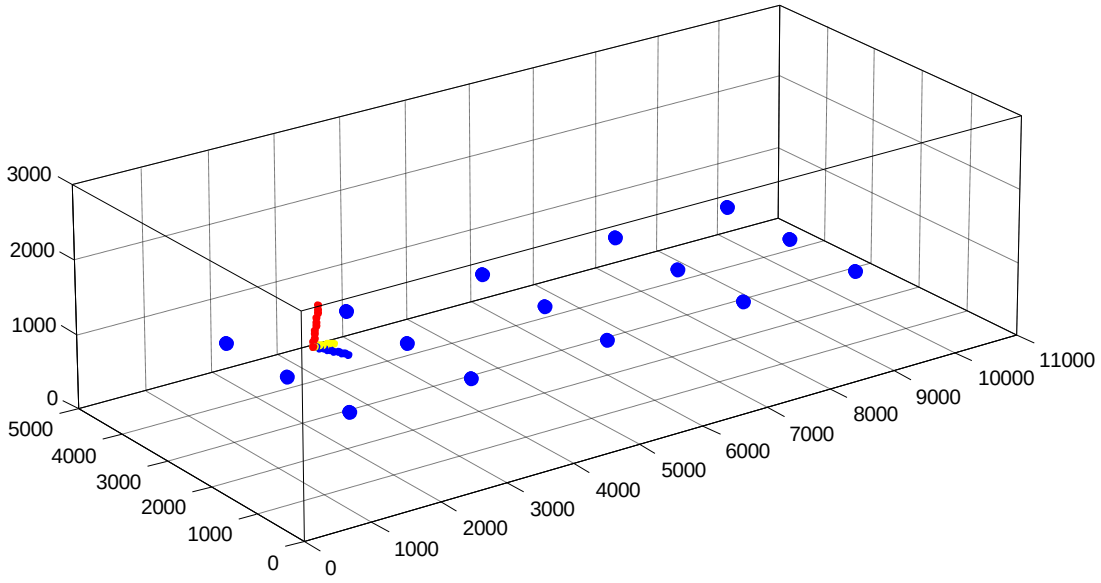

Figure 5.4. Calibration point locations and base station location in the simulation environment. The dimensions are in mm.

$$\propto = \tan^{-1}\frac{p_x}{p_y} \tag{5.27}$$

$$\beta = \tan^{-1}\frac{p_z}{\sqrt{p_x^2 + p_y^2}} \tag{5.28}$$

The calibration points projected to the image plane from the Angle of Arrival data (see Fig. 5.6) was calculated by

$$\mathrm{x_{im}} = f \tan \propto \tag{5.29}$$

$$\mathrm{z_{im}} = \sqrt{\mathrm{x_{im}^2} + f^2}\ \tan\beta \tag{5.30}$$

where the focal length *f* was set at a 6 mm, in practice this has no effect to the results.

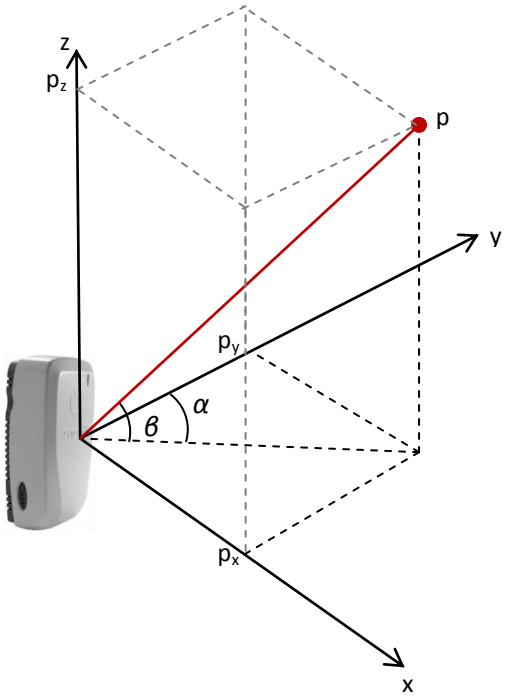

Figure 5.5 Conversion to angles (α = azimuth, β = elevation) from a calibration point *p*

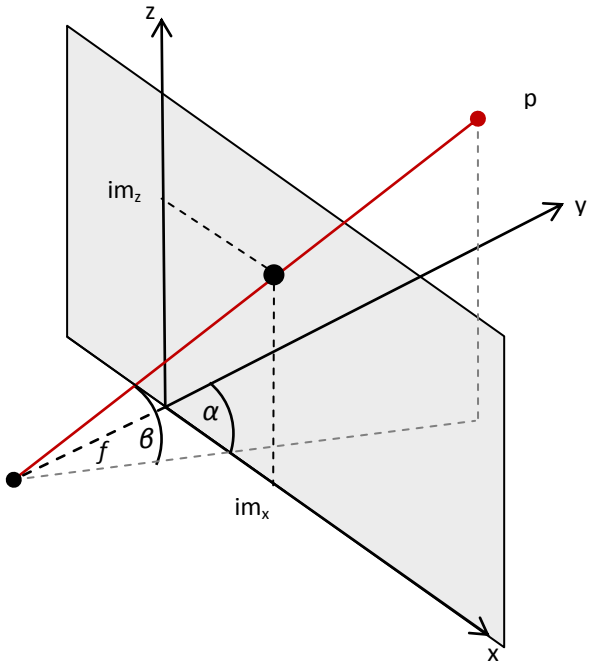

Figure 5.6 A calibration point projection to the image plane

In order to understand the noise characteristics of Ubisense data, a series of experiments were performed. Horizontal and vertical angle variations were studied for a static tag by gathering AOA data across the whole measured volume. Figure 5.7 shows the histogram from all data set. The 1st standard deviations are between 0.01 and 0.02 radians for both azimuth and elevation angles in the experiments. The large variations in the data were mainly caused by tag locations at the boundary angles of the sensor (± 65 degrees in azimuth and ± 50 degrees in elevation).

Simulation tests for the base station calibration algorithm were run so that 100 data samples per calibration points were generated with additive sensor noise modelled with a normal distribution. The noise level (1st std deviation) was set to 0.01 radians and 0.02 radians, both for azimuth and elevation angles (see Fig. 5.7). A median filter was applied to filter out the noisy data. 15 filtered image plane locations were used as inputs for the base station pose estimation algorithm. This scenario was run 100 times and cumulative figures were created from the residual errors. The effects of the shape of the calibration pattern were also tested.

The pattern was modified by systematically reducing points starting from the edges, from 15 points to three so that the points filled the image plane as widely as possible.

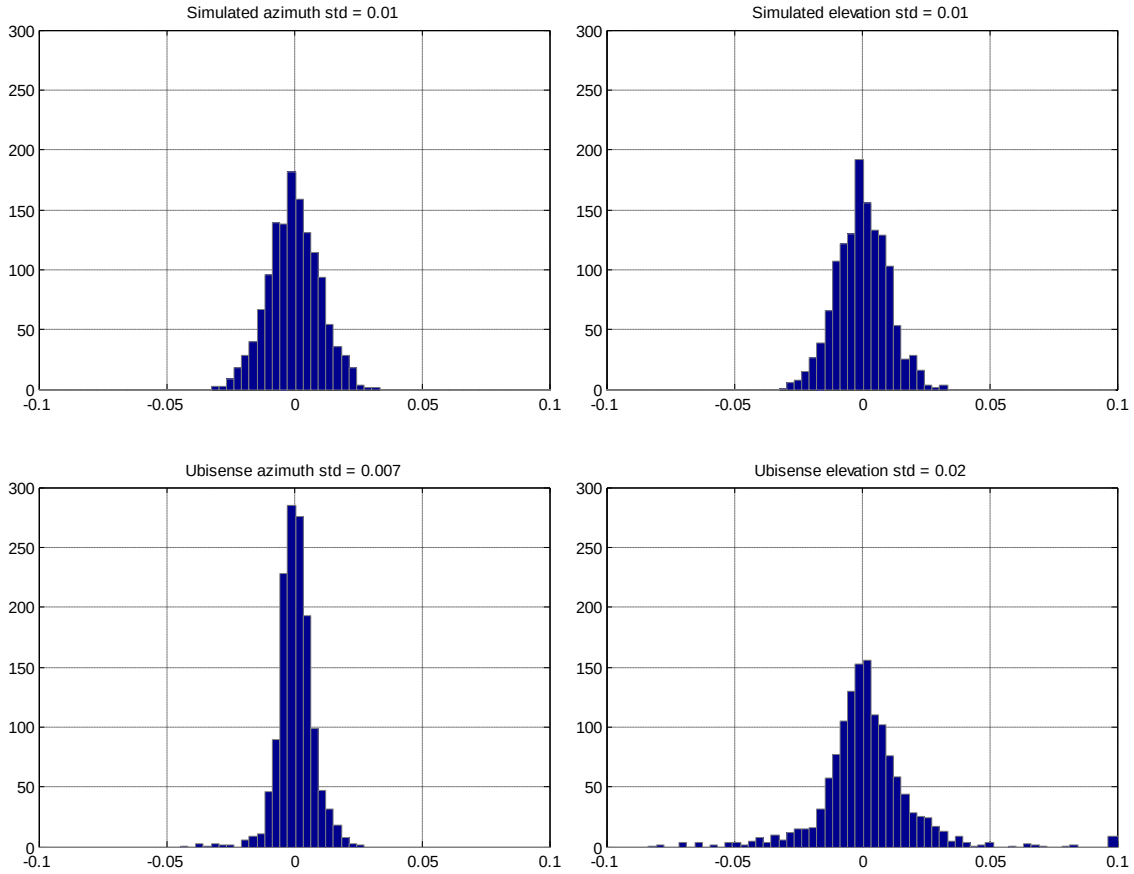

Figure 5.7. Distribution of AoA measurements: real measurements (lower) and comparable distributions used in the simulation tests (upper).

Figure 5.8 shows the distribution of pose estimation error for a single base station. The first estimation chart is for position and the second is for orientation. The figure describes how accurately the algorithm can compute the location and the orientation parameters for a single sensor in respect of amount of calibration points used.

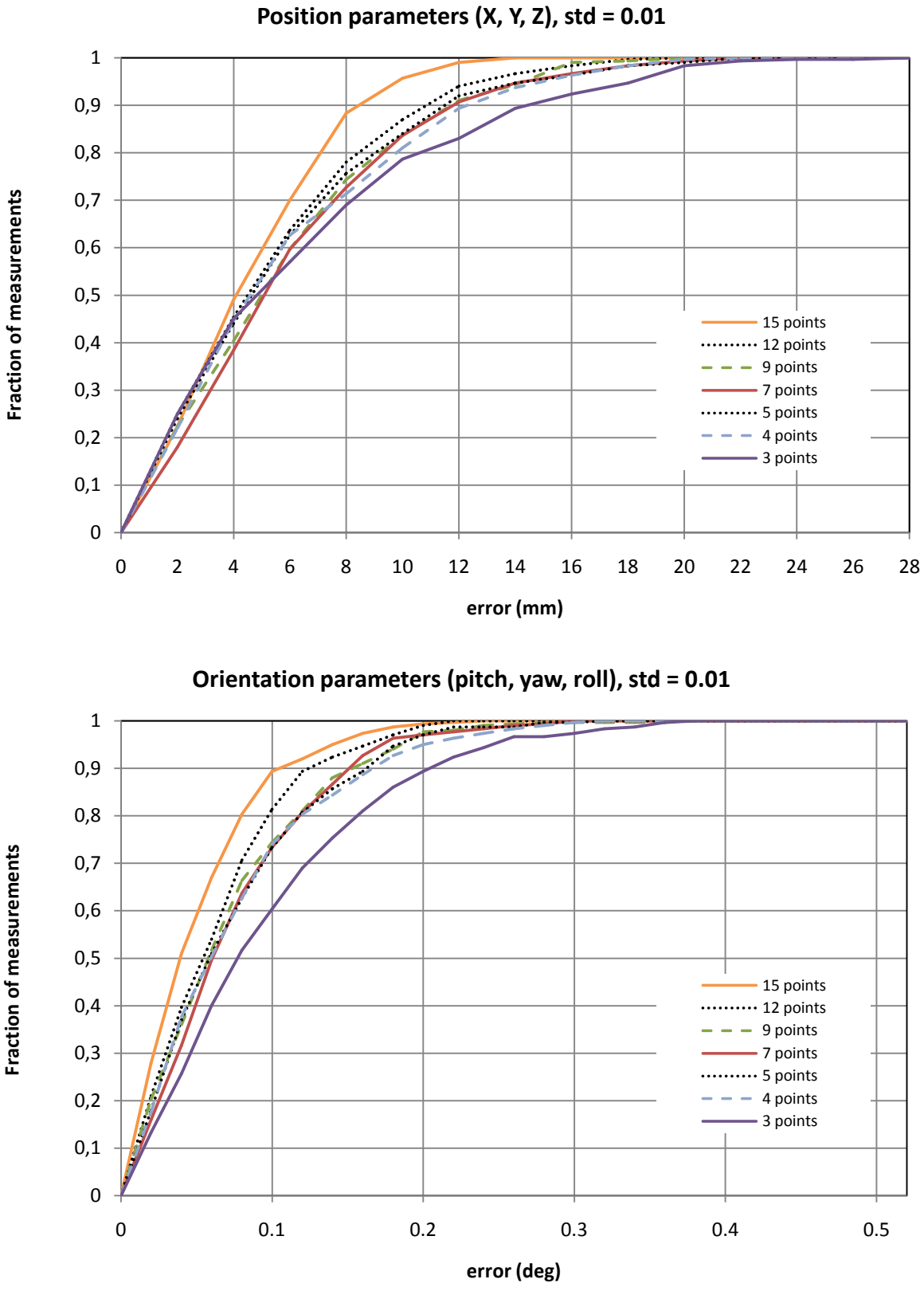

Figure 5.8. Estimation errors of the calibration algorithm with different shapes and sizes of the calibration point sets. 1st standard deviation of AoA measurements was set 0.01 radians.

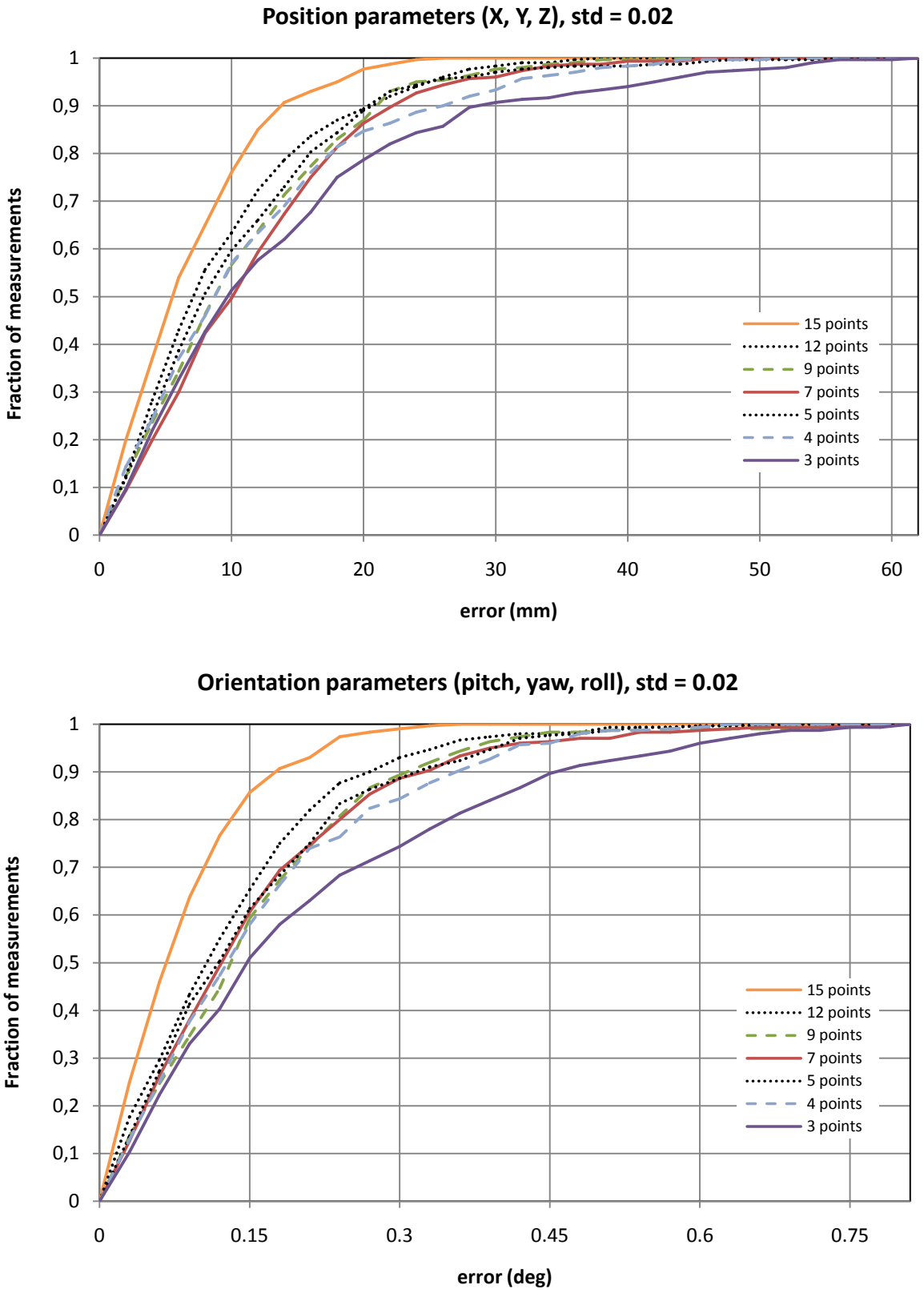

Figure 5.9. Estimation errors of the calibration algorithm with different shapes and sizes of the calibration point sets. 1st standard deviation of AoA measurements was set 0.02 radians.

The distribution graphs show, for instance, that with four calibration points on a planar mesh, and 100 of angular measurements per node with additive noise of 0.01 radian, calibration accuracy of a single sensor at the level of 15 mm and 0.2 degrees can be achieved at 95 % confidence level. Tables 5.1 and 5.2 summarise the simulation test results. This calibration error remains as a systematic error per base station while finally tracking located objects with the RTLS system.

Table 5.1 Estimation error of position parameters at 95 % confidence level

	std 0.01	*std 0.02*
15 points	10 mm	18 mm
7 points	14 mm	27 mm
4 points	15 mm	31 mm
3 points	18 mm	42 mm

Table 5.2 Estimation error of orientation parameters at 95 % confidence level

	std 0.01	*std 0.02*
15 points	0.14 deg	0.22 deg
7 points	0.17 deg	0.39 deg
4 points	0.2 deg	0.41 deg
3 points	0.25 deg	0.58 deg

5.2.4. Internal Calibration Experiment

The Angle of Arrival measurements seem to have similar systematic errors as optics in camera based systems. It is most likely due to the antenna's properties. We took a practical approach for this, and created a static map from measured AOA values to corrected ones. The map was created using a test mesh located in a wall (see Fig. 5.10), where reference locations were set within constant intervals of azimuth and elevation angles. The accurate values of the reference coordinates (and angles) were recorded using a Total Station (or Tachymeter) and a base station. Total station is an electronic/optical instrument used in modern surveying. The base station was placed and orientated in a similar way as the Total Station by 1 cm level of accuracy, which was a fair requirement with regards to the accuracies of the AOA measurements. The test mesh covered a field of view of the sensor of about 85 degrees in azimuth and 45 degrees in elevation.

Figure 5.11 shows the data recorded by the base station (red circles) and the Total Station (blue circles). There seem to be a radial distortion, which seems to be strongest at the fringe area of the measurement space. The blue circles are real locations in a reference plane, and

the red circles are corresponding measured locations in the reference wall. The red locations were calculated from the measured AOA measurements and should be corrected to match corresponding blue dots. The correction map can be used in measurements by correcting the measured angles according to the map. The connected points of the correction map are used for the measurement with linear interpolation between the reference and measured points.

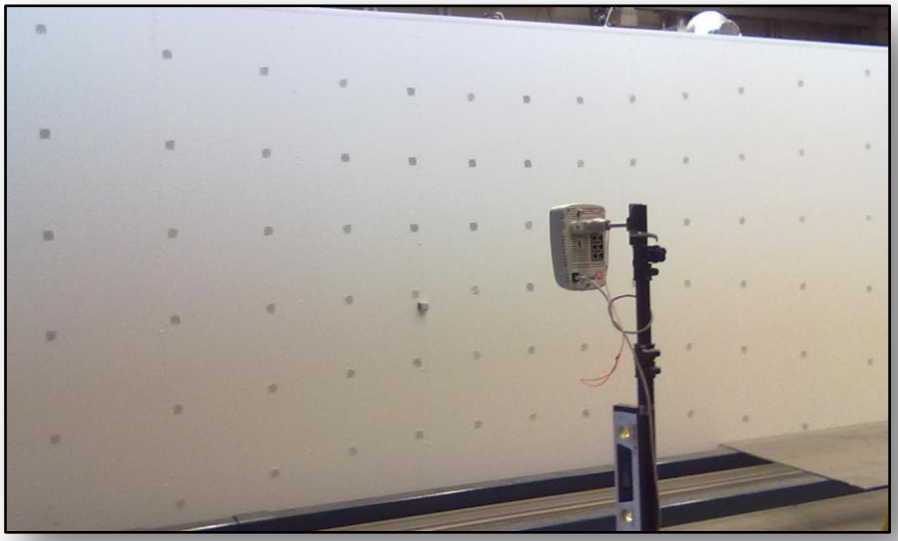

Figure 5.10. Test environment for internal calibration experiment

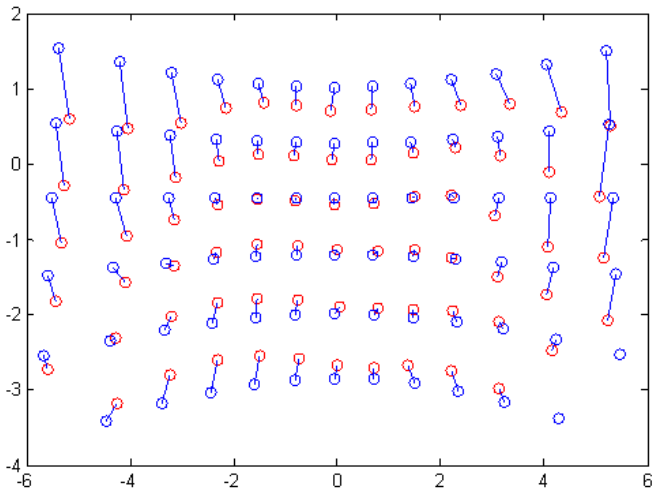

Figure 5.11. Correction map for the AOA measurements

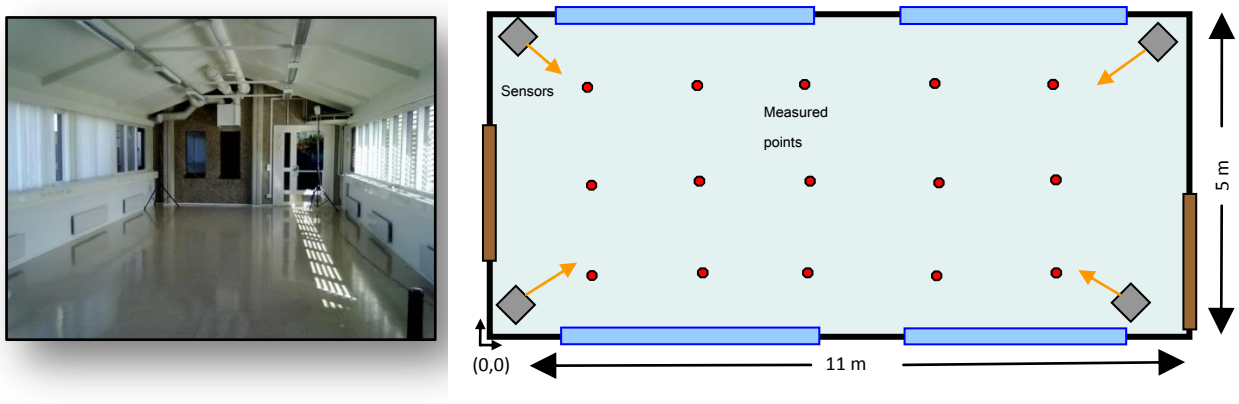

Figure 5.12. Test environment for external calibration experiment

5.2.5. External Calibration Experiment

The calibration algorithm was evaluated in practice using the Ubisense Real Time Location System. The test set-up consists of four base stations and 15 calibration points (see Fig. 5.12). The simulated and real experiment differed in their source of input data. For simulated case, data were generated given the tag–sensor positions and the noise model. For real experiments, data were gathered from continuous AOA sensor readings by setting the tag to each calibration point for some time, where the tag was at 0.91 cm height. The angular measurement data was pre-processed with median filter to remove poor outlying measurements.

The algorithm requires rough initial position and orientation parameters for the base station. In the experiment, the algorithm converged when the initial parameters deviated from the estimated values less than 1 meter for each X, Y and Z and 30 degrees for pitch and yaw. Roll was set to 0 degrees which was close to the estimated angle. However, the magnitude of the deviation depends on the pattern and the amount of calibration points used. In general, roll can be easily guessed in 10 degrees accuracy and pitch and yaw in 20 degrees accuracy. For positions, Z can be usually measured in 50 cm accuracy, but X and Y can be more troublesome.

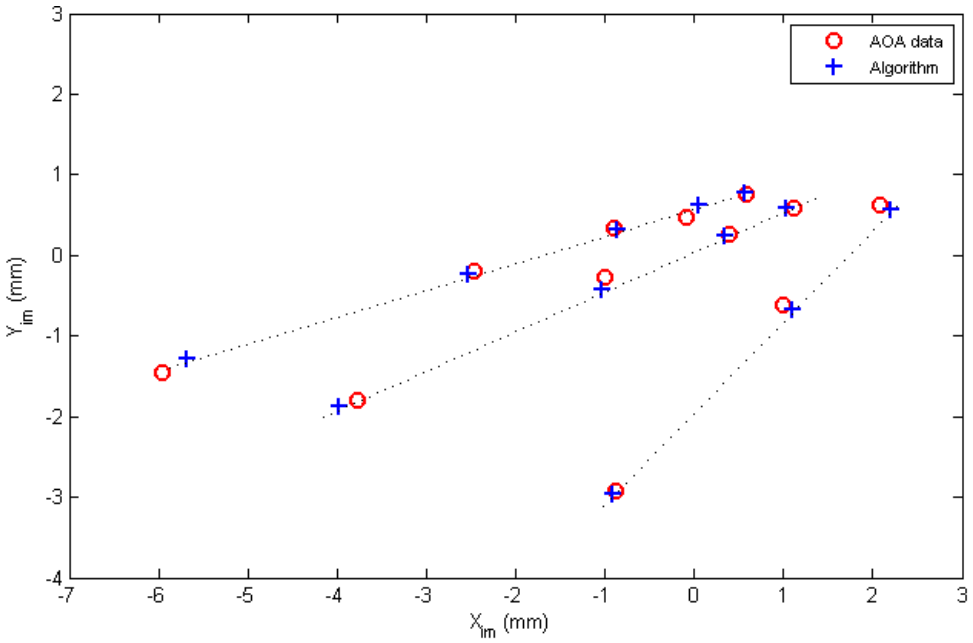

Figure 5.13. Fit of the known calibration points to the AOA measurements

Results from applying our calibration algorithm for one base station are shown in Figure 5.13. Some of the faulty sensor readings were removed or corrected with the correction map. The fit of the measured and nominal points is good.

The Table 5.3 shows the calibration parameters used for each sensor in the experiment measurement. For reference, also the Ubisense's proprietary calibration method was tested. The meaning of the parameters and calibration methods are explained in Chapter 4.1.

In addition to the previous calibration settings, a manual "Displaced" calibration setting was taken into the comparison. The idea was to compare how much manual inaccurate survey for the calibration affects the final accuracy of the system. This was done by using input values in the location platform with deviations of 10 cm in X and Y axes and 5 cm in Z axis from the surveyed values. Finally, the Ubisense calibration was performed to a single point at the boresight of all sensors.

It should be noted, that for "Single Point" and "Multi Point Median" only the orientation (pitch and yaw) and the cable offset of the base station is estimated. The location coordinates from the manual survey were used.

Table 5.3. Calibration parameters used in the external calibration measurements

Sensor 1	*Single calibration*	*Median calibration*	*Algorithm*	*Displaced*
X (mm)	470	470	420	520
Y (mm)	430	430	330	470
Z (mm)	2250	2250	1980	2300
Pitch (deg)	-15.4	-17.3	-13.5	-18.3
Yaw (deg)	24.9	25	26.2	27.1
Roll (deg)			3.4	

Sensor 2	*Single calibration*	*Median calibration*	*Algorithm*	*Displaced*
X (mm)	410	410	340	310
Y (mm)	4350	4350	4400	4500
Z (mm)	2360	2360	2260	2300
Pitch (deg)	-18.7	-21.1	-20.3	-17.1
Yaw (deg)	-25.8	-26.3	-25.7	-26.9
Roll (deg)			-1.9	
Cable offset	337.1	338.2	338.2	336

Sensor 3	*Single calibration*	*Median calibration*	*Algorithm*	*Displaced*
X (mm)	10100	10100	10190	10000
Y (mm)	770	770	730	920
Z (mm)	2420	2420	2430	2370
Pitch (deg)	-17.5	-18.6	-18.1	-16.2
Yaw (deg)	158.9	158.9	158.1	159.5
Roll (deg)			0.8	
Cable offset	335.9	336.8	336.8	335.8

Sensor 4	*Single calibration*	*Median calibration*	*Algorithm*	*Displaced*
X (mm)	10350	10350	10430	10250
Y (mm)	4690	4690	4730	4840
Z (mm)	2300	2300	2170	2350
Pitch (deg)	-14.7	-15.6	-13.8	-14.3
Yaw (deg)	-152.4	-152.2	-153	-151.3
Roll (deg)			0.1	
Cable offset	1425.6	1425.9	1425.9	1427

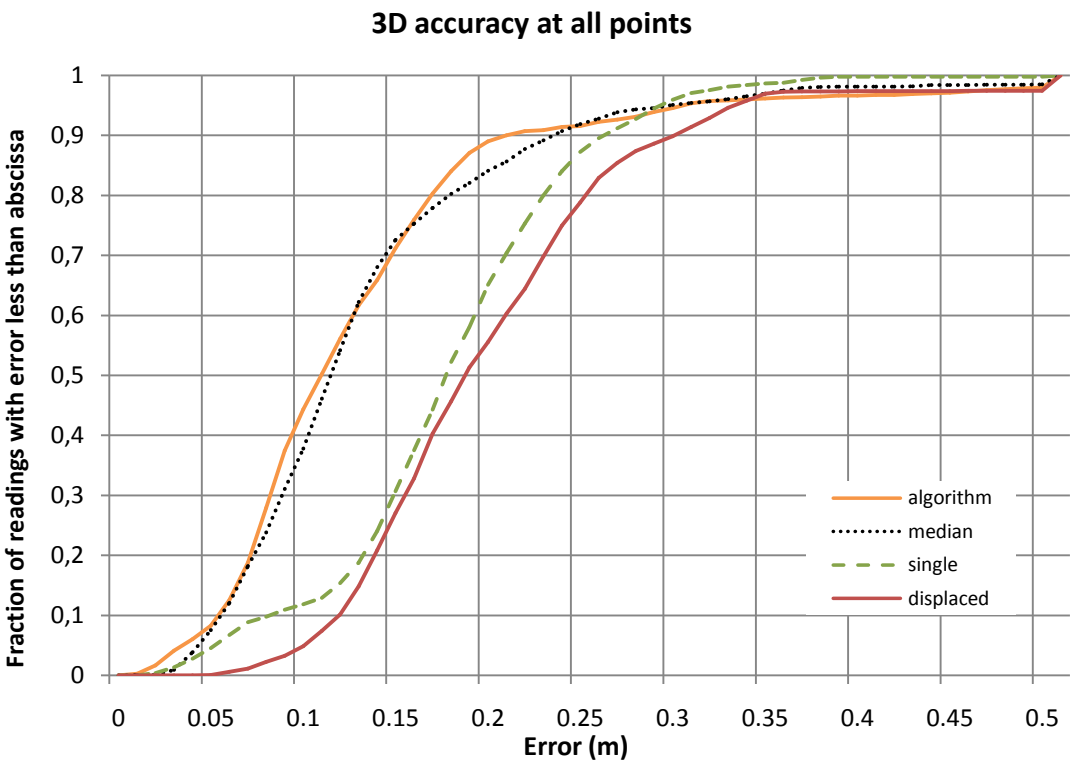

Figure 5.14. 3D accuracy of the Ubisense RTLS by using different calibration settings.

Figure 5.14 compares the Ubisense RTLS 3D-accuracy by using parameter settings resulted from calibrations in Table 5.3. In the figure "single" is the Ubisense's one point calibration method, "median" is a process where "single" calibration has been applied over the whole measured volume and "algorithm" is our algorithm. It can be seen, that by applying the calibration algorithm, the final accuracy of the positioning system can be improved, in this case to 21 cm at 90% confidence.

5.3. Conclusion

In this chapter two calibration methods suitable for UWB were presented. A pseudoranging calibration which utilises the Time-difference of Arrival information of the positioning system. And a calibration algorithm model which utilises Angle of Arrival information (*flexible calibration*). The pseudoranging calibration was not further implemented in the thesis as the Ubisense's internal access limitations restricted the use the of the TDOA information.

The chapter mainly focused on the research of implementing calibration algorithm of cameras for UWB positioning system. The implemented flexible calibration algorithm needs rough initial parameters for the position and orientation of the base station and at least three known points in the measured space. The accurate position and orientation of the base station is then computed iteratively. In comparison, the Ubisense's proprietary calibration method needs accurate positions of all the base stations and at least one known point in the measured space. The orientation of the base station is crucial as the roll orientation has to be set accurately to 0 degrees. The automated calibration in the software then computes the orientation of the base stations (yaw and pitch).

Because of more flexible calibration, positioning accuracy of the Ubisense system was as whole in average better; this is mainly due to the more precise position and orientation of the base station. Simulation and experiment studies showed that camera calibration method can be successfully adapted to position systems based on UWB technology.

6. CONCLUDING REMARKS

This thesis covered some concepts related to indoor positioning using UWB as well as some of the most common wireless estimation techniques in RF positioning. In estimation techniques Time-based estimation and Angle of Arrival are very well suited in UWB positioning.

Hardware and software procured from Ubisense was researched. The Ubisense RTLS bases on UWB technology and utilises Angle of Arrival and Time Difference of Arrival techniques. Performance measurements were done in various environments. The Ubisense RTLS performed well in different radio environments and positioning accuracy is sufficient for many indoor positioning applications, such as, patient monitoring in health care or asset tracking.

Algorithms for calibrating a variety of systems utilising pseudoranging and/or Angle of Arrival estimation techniques were introduced. The foundation of the thesis is the presented and implemented calibration algorithm utilising Angle of Arrival readings in Chapter 5. The algorithm bases on pin-hole camera model and is implemented to UWB positioning system. An implementation of the algorithm and evaluation of its effectiveness both in simulations and in practice was presented. The simulated and real experiment differed in their source of input data. For simulated case, data were generated given the tag–sensor positions and the noise model. For real experiments, data were gathered from continuous AOA sensor readings of a stationary tag. We also presented study of AOA data obtained from Ubisense, preprocessing and prefiltering the raw data to get better and more robust estimates.

The algorithm does not require accurate placing of base stations or setting their orientations though rough initial parameters are needed. Because of the flexibility the installation setup time is reduced and made easier. In our experimental test the final accuracy of the system improved a little.

According to the measurement results in the Chapter 4, the Ubisense should be calibrated using multiple calibration points (eg. multi-point median). Then, the calibration algorithm requires less work compared to the Ubisense’s proprietary calibration as no base stations need to be surveyed.

Although the main focus is on UWB system, the calibration algorithm is not limited to UWB and should be able implement to other position technology using AOA-like information or non-radio systems

Some example applications which would particularly benefit from the flexible calibration are deployments where the positioning system has to be installed and set-up quickly, or where the accurate surveying of tag positions can be easier than the base stations. It would also benefit deployments where no advanced measuring tools are available. One good deployment example for the flexible calibration would be indoor sports court where the sensors would be installed quickly (for example with tripods) and then use the markings on the court for the known tag positions. Another example is a dynamic deployment where the tracked environment changes constantly, for example, inside mines. Some deployments would also benefit from larger field of view in vertical bearings that would be utilised by rotating the base station 90 degrees in roll and the calibration would compute the accurate orientation for all three rotations.

One interesting idea for hybrid calibration would be utilising both the pseudoranging (TDOA) and AOA data for two-phased calibration. Firstly, the system would be calibrated with the pseudoranging calibration which computes rough positions for the base stations. Secondly, the flexible calibration algorithm would be used to calculate the more accurate positions and orientations for the base stations. This would eliminate the need of initial position parameters for the algorithm. The calibration algorithm would still require rough initial parameters for the orientation, but with increased flexibility. Unfortunately we did not have access to the TDOA data of the Ubisense system.

7. REFERENCES

Arslan, H., Chen, N.Z. and Di Benedetto, M. (2006). Ultra Wideband Wireless Communication, Wiley.

Bahl, P. and Padmanabhan, V.N. (2000). RADAR: An In-Building RF-Based User Location and Tracking System, *Proceedings of IEEE Infocom 2000.*

Caffery, J.J. (1999). Wireless Location in CDMA Cellular Radio Systems, Springer.

Commission of the European Communities (2007). Commission decision on allowing the use of the radio spectrum for equipment using ultra-wideband [Online] [cited Dec 2009]. Available: http://eur-lex.europa.eu/LexUriServ/LexUriServ.do?uri= CONSLEG:2007D0131:20090630:EN:PDF

Discrete Time Communications (2002). "New" Ultra-wideband technology white paper.

Duff, P. and Muller, H. (2003). Autocalibration algorithm for ultrasonic location systems. Proceedings of the Seventh IEEE International Symposium on Wearable Computers, 62-68. IEEE Computer Society.

Duff, P.A. (2008). Auto-Calibration for Ultrasonic Positioning Systems, University of Bristol.

ECMA International (2008). Standard ECMA-368 High Rate Ultra Wideband PHY and MAC Standard.

Ekahau Incorporated (2010). [Online] [cited Apr 2010]. Available: http://www.ekahau.com

FCC Federal Communications Commission (2002). First Report and Order 02-48. [Online]. [cited Dec 2009] Available: https://ipo.llnl.gov/data/assets/docs/FCC_rules.pdf

FCC Federal Communications Commission (2006). Part 15 - Radio Frequency Devices. [Online] [cited Mar 2010]. Available: http://www.gpo.gov/fdsys/pkg/CFR-2009-title47-vol1/pdf/CFR-2009-title47-vol1-part15.pdf

Gezici, S. (2008). A Survey on Wireless Position Estimation. *Wireless Personal Communication* 44, 263–282.

Ghavami, M., Michael, L.B. and Kohno, R. (2004). ultra wideband signals and systems in communication engineering, Wiley.

Hämäläinen, M. (2006). Singleband UWB Systems Analysis And Measurements of Coexistence, Univeristy of Oulu.

Heikkila, T., Sallinen, M., Matsushita, T. and Tomita, F. (2002). Flexible hand-eye calibration for multi-camera systems, Intelligent Robots and Systems, 2000. (IROS 2000). *Proceedings. 2000 IEEE/RSJ International Conference on.*

Heikkila, T., Koskinen T., Lehikoinen T. (2010). Flexible Calibration of Base Stations for Real Time Location Systems based on angle-of-arrival measurements, *Ubisense User Group Conference 2010*.

IEEE Computer Society (2007). Part 15.4: Wireless Medium Access Control (MAC) and Physical Layer (PHY) Specifications for Low-Rate Wireless Personal Area Networks (WPANs) Amendment 1: Add Alternate PHYs.

Immoreev, I. and Sinyavin, A.N. (2002). Features of ultra-wideband signals' radiation*, IEEE Conference on Ultra Wideband Systems and Technologies, 2002*. Digest of Papers.

Kohno, R. (2006). Interpretation and future modification of Japanese regulation for UWB*, IEEE P802.15-06/261r0.*

Lowe, D. (1985). Perceptual organisation and Visual Recognition. Kluwer Academic Publishers Norwell, MA, USA.

Mallat, A., Louveaux, J. and Vandendorpe, L. (2007). UWB based positioning in multipath channels: CRBs for AOA and for hybrid TOA-AOA based methods, *Proc. IEEE Int. Conf. on Commun. (ICC).*

Oppermann, I., Hämäläinen, M. and Iinatti, J. (2004). UWB Theory and Applications, Wiley.

Paul A., Wan E. (2009) RSSI-Based Indoor Localization and Tracking Using Sigma-Point Kalman Smoothers. IEEE Journal of Selected Topics in Signal Processing, 3: 860 – 873.

Poor, H.V. (1994). An Introduction to Signal Detection and Estimation , Springer.

Remondino, F. and Fracer, C. (2006). Digital Camera Calibration Methods: Considerations and Comparisons, ISPRS Commission V Symposium on Image Engineering and Metrology, IAPRS.

Sahinoglu, Z., Gezici, S. and Güvenc (2008). Ultra-wideband Positioning Systems: Theoretical Limits, Ranging Algorithms, and Protocols, Cambridge University Press.

Siwiak, K. and McKeown, D. (2004). ultra-wideband radio technology, Wiley.

Svensson, A. (2004). Introduction to and some results on DS-UWB, multiband UWB and multiband OFDM [Online] [cited Jan 2010]. Available: http://www.signal.uu.se/Research/PCCWIP/Visbyrefs/Svensson_Visby04.pdf

Time Domain (2010). [Online] [cited Jun 2010]. Available: http://www.timedomain.com/

Tsai, R.Y. (1986). An Efficient and Accurate Camera Calibration Technique for 3D Machine Vision., *Proceedings of IEEE Conference on Computer Vision and Pattern Recognition*.

Turin, G. (1960). An introduction to matched filters, *IRE Transactions on Information Theory*.

Ubisense Ltd (2010). [Online] [cited Jun 2010]. Available: http://www.ubisense.net

Wang, Y., Jia, X., Lee H.K. and. Li G.Y. (2003). An indoor wireless positioning system based on WLAN infrastructure*. 6th International Symposium on Satellite Navigation Technology Including Mobile Positioning & Location Services.*

Wimedia Alliance (2009). Worldwide regulatory status [Online] [cited Jan 2010]. Available: http://www.wimedia.org/en/resources/worldwide_regulatory.asp

ZeroOne (2007). Roll, yaw and pitch axis definition for an airplane [Online] [cited Aug 2010]. Available: http://en.wikipedia.org/wiki/File:Flight_dynamics_with_text.png

Zhang, Y., Partridge, K. and Reich, J. (2007). Localizing Tags Using Mobile Infrastructure, *Location- and Context-Awareness, Lecture Notes in Computer Science.*